Compositional Engineering of Environment Friendly Absorber Layer for Perovskite Solar Cells

By

Abdul Sattar

Reg # 00000273332

Session 2018-20

Supervised by

Dr. Nadia Shahzad

US-Pakistan Center for Advanced Studies in Energy (USPCAS-E)

National University of Sciences and Technology (NUST)

H-12, Islamabad 44000, Pakistan

June 2022

Compositional Engineering of Environment Friendly Absorber Layer for Perovskite Solar Cells

By

Abdul Sattar

Reg # 00000273332

Session 2018-20

Supervised by

Dr. Nadia Shahzad

A Thesis Submitted to the US-Pakistan Center for Advanced Studies in Energy in partial fulfillment of the requirements for the degree of MASTER of SCIENCE

in

ENERGY SYSTEMS ENGINEERING

US-Pakistan Center for Advanced Studies in Energy (USPCAS-E)

National University of Sciences and Technology (NUST)

H-12, Islamabad 44000, Pakistan

June 2022

THESIS ACCEPTANCE CERTIFICATE

Certified that final copy of MS thesis written by **Mr. Abdul Sattar**, (Registration No. 00000273332), of U.S.-Pakistan center for Advanced Studies in Energy has been vetted by undersigned, found complete in all respects as per NUST Statues/Regulations, is within the similarity indices limit and is accepted as partial fulfillment for the award of MS degree. It is further certified that necessary amendments as pointed out by GEC members of the scholar have also been incorporated in the said thesis.

Signature: _____

Name of Supervisor: Dr. Nadia Shahzad

Date: _____

Signature (HoD): _____

Date: _____

Signature (Dean/Principal): _____

Date: _____

CERTIFICATE

This is to certify that work in this thesis has been carried out by **Mr. Abdul Sattar** and completed under my supervision in Solar Energy Research Laboratory, US-Pakistan Center for Advanced Studies in Energy (USPCAS-E), National University of Sciences and Technology, H-12, Islamabad, Pakistan.

Supervisor: _____

Dr. Nadia Shahzad
USPCAS-E, NUST,
Islamabad

GEC member # 1: _____

Dr. Muhammad Imran Shahzad
NS & TD,NCP,
Islamabad

GEC member # 2: _____

Dr. Rabia Liaquat
USPCAS-E, NUST,
Islamabad

GEC member # 3: _____

Dr. Majid Ali
USPCAS-E, NUST,
Islamabad

HoD- ESE: _____

Dr. Rabia Liaquat
USPCAS-E, NUST,
Islamabad

Principal/ Dean: _____

Prof. Dr. Adeel Waqas
USPCAS-E, NUST,
Islamabad

Dedication

*To My Late Father, **Munawar Hussain**, Your Presence I Will Always Miss!*

Acknowledgments

First and foremost, I would like to thank **Almighty ALLAH** who is the creator of everything and who says, **كُن فَيَكُونُ** *(Be, and it is!***).** All respects for His **Prophet Muhammad** (PBUH, On Whom Be ALLAH'S Blessings and Salutations). In fact, without His blessings, this difficult and diligent task would have been impossible.

I would like to acknowledge and give my warmest thanks to my supervisor, **Dr. Nadia Shahzad**, who made this work possible. Her guidance and advice carried me through all the stages of conducting this research work. I am very grateful to my supervisor for providing me the freedom of executing research ideas and for her support in building my research intuition.

I take this opportunity to express gratitude to all of the Department faculty members for their help and support. I would like to extend my special thanks to all the lab engineers for their guidance during my work. I would also like to thank my lab fellows for their continuous support and encouragement during long work hours at the Solar energy research lab.

I pay my regards to my GEC members for their utmost support and guidance throughout this research project. I am also grateful to USPCAS-E, for allowing me to use their lab facilities.

Abdul Sattar

Abstract

Lead halide-based perovskite solar cells (PSCs) have become a popular choice to dethrone existing silicon-based photovoltaic technology due to their skyrocketing efficiencies and low-cost fabrication techniques. However, as they are racing for commercialization, lead toxicity is a major obstacle standing in the way hampering their large-scale manufacturing. Recently, tin-lead (Sn-Pb) mixed perovskites have gained unprecedented attention to mitigate lead toxicity along with obtaining outstanding power conversion efficiencies. But, since with every blessing comes a burden, unfortunately, Sn-Pb mixed perovskite materials have inherited two fundamental problems from their predecessors, tin perovskites: i) facile Sn^{+2} oxidation and ii) uncontrolled fast crystallization leading to the significant loss of PSCs device performance. To counter this, herein, additive engineering has been applied to ameliorate structural, optoelectronic, and morphological properties of Sn-Pb mixed perovskites. A Lewis base, caffeine (1,3,7-trimethylpurine-,2,6-dione), containing two carbonyl functional groups (C=O), is introduced which has also been extensively studied as an antioxidant in food and biotechnology. Control and caffeine doped Sn-Pb perovskite precursors were prepared and spin-coated onto the glass substrates to prepare perovskite films. The prepared Sn-Pb perovskite films were studied using advanced characterizations techniques, *i.e.*, X-ray diffraction, UV-visible spectroscopy, photoluminescence spectroscopy, Fourier transform infrared spectroscopy, electrochemical impedance spectroscopy, and scanning electron microscopy. The results indicate that caffeine-doped Sn-Pb perovskite films showed enhanced crystallinity, reduced trap-state density, and increased grain size implying superior structural, optoelectronic, and morphological properties as relative to the undoped Sn-Pb perovskites.

Keywords: *Ambient fabrication, Tin-Lead mixed perovskites, Narrow bandap, Lead mitigation*

Table of Contents

List of Figures

List of Tables

List of Publications

Journal Publicaitons.

1. **Abdul Sattar**, Nadia Shahzad, Muhammad Ali Tariq, Tanzeela Yousaf, Muhammad Salik Qureshi, Muhammad Imran Shahzad, Rabia Liaquat, Majid Ali, "**Carbonyl functional group assisted crystallization of mixed tin-lead narrow bandgap perovskite absorber in ambient conditions**", Applied Physics Letters ***(****Under Review)*
2. **Abdul Sattar**, Nadia Shahzad, Muhammad Ali Tariq, Tanzeela Yousaf, , Muhammad Imran Shahzad, Rabia Liaquat, Majid Ali, Zuhair S. Khan, Federico Bella, "**Unravelling the Role of Bifunctional Additives Towards Realization of Highly Efficient and Environmentally Robust Tin Halide Perovskite Solar Cells**", Energy and Environmental Materials *(Submitted)*
3. Muhammad Ali Tariq, Nadia Shahzad, **Abdul Sattar,** Muneeza Ahmad, Mustafa Anwar, Muhammad Imran Shahzad**.** "**Role of bi-layered CuSCN based hole transport films to realize highly efficient and sable perovskite solar cells**". *Surfaces and Interfaces.* https://doi.org/10.1016/j.surfin.2021.101657
4. M. Ahmad, N. Shahzad, M.A. Tariq, **Abdul Sattar**, D. Pugliese, "**Investigating the Sequential Deposition Route for Mixed Cation Mixed Halide Wide Bandgap Perovskite Absorber Layer**", Énergies. https://doi.org/10.3390/en14248401
5. Muhammad Ali Tariq, Nadia Shahzad, **Abdul Sattar**, Tanzeela Yousaf, Ahad Hussain Javed, Naseem Iqbal, Muhammad Imran Shahzad**. "Highly stable and efficient NH3(aq)/DES processed CuSCN bilayers for perovskite solar cells".** Materials Chemistry and Physics *(Submitted)*
6. Tanzeela Yousaf, Nadia Shahzad, **Abdul Sattar**, Muhammad Ali Tariq, Naveed Hussain, Zuhair S. Khan, Sofia Javed, Muhammad Imran Shahzad, " **Fabrication of Low-cost carbon based PSCs using compositional engineering of perovskite absorber material in ambient conditions**", Thin Solid Films *(Submtted*

Poster Presentation.

- **Abdul Sattar**, Tanzeela Yousaf, Nadia Shahzad, Ahad Hussain Javed, Muhammad Imran Shahzad ***Transport Layer Free Carbon-based Perovskite Solar Cells****",* 21-22 September 2021 International Workshop on Nanomaterials for Energy Conversion, Emerging Photovoltaic and Optoelectronic Technologies (NEEPO-21), National Centre for Physics, Islamabad (46000), Pakistan

List of Abbreviations

GHGs	Greenhouse gasses
LPSCs	Lead based perovskite solar cell
THPSCs	Tin halide based perovskite solar cells
J_{SC}	Short circuit current density
V_{OC}	Open circuit voltage
FF	Fill-factor
PCE	Power conversion efficiency
FA	Formamidinium
MA	Methylammonium
FTO	Fluorine doped tin oxide
RT	Room temperature
TCO	Transparent conductive oxide
HTL	Hole transport layer
ETL	Electron transporting layer
PTAA	Poly(triarlyamine)
X_3	Halides
DSSCs	Dye sensitized solar cells
PCBM	Phenyl-C61-butyric acid methyl ester
BCP	Bathocuproine
PSKT	Perovskite
meso	Mesoporous
ITO	Indium tin oxide
Au	Gold

Chapter 1 Introduction

This chapter discusses the background, importance, and need for solar photovoltaic technology as a tool to harvest energy from the Sun. Sun has remained a continuous source of energy making life possible on planet earth since its inception. However, for the last two hundred years, the industrial revolution has disrupted the balance of the entire ecosystem resulting in climate change and global warming, frequent droughts etc.

1.1 Fossil fuel consumption and climate change

Fossil fuels (Coal, Gas, and Oil) constitute a basic component in the energy sector of the world. They are used extravagantly in every energy-dependent domain of daily life. Primarily, Coal is utilized in the power sector to produce electricity from thermal energy stored in the coal. Whereas Gas is consumed in the heating domestic and industrial sectors as well for electricity production. Furthermore, it is used as a fuel in the transport sector. In the same way, the transport sector also relies heavily upon Oil that is being used excessively as a fuel to power automobiles. Since these resources are limited. Therefore, it is the undeniable truth that one day they will be going to diminish. The limited availability of fossil energy fuels is a serious global concern. Moreover, they have been a continuously growing source of global warming and CO_2 emissions. For the year 2021, according to the energy outlook report, for the first time in the last 50 years, the highest economic growth up to 6% is observed majorly relying upon the consumption of fossil fuels resulting in the second-largest increase of CO_2 and greenhouse gasses (GHGs) emissions in the world's history. As a result of the intense consumption of fossil fuels, unprecedented wavering weather conditions were recorded i.e., some countries were faced with extreme weather conditions like floods, etc. and others were faced with drought conditions for the year 2021.[1]

In addition, British petroleum has reported that fossil fuels are holding major share in the current world energy consumption mix. Oil is considered as the biggest contributor having share more than 31.2% followed by coal and natural gas holding 27.2% and 24.7% share, respectively. On the other hand, renewables have a very low share of energy to the current world energy constituting approximately 5.7% of the current world energy mix consumption.[2] As a result, these fossil fuels are also major contributor to the annual GHG and CO_2 emissions destroying the natural balance of the ecosystem for hundreds of years.[3]

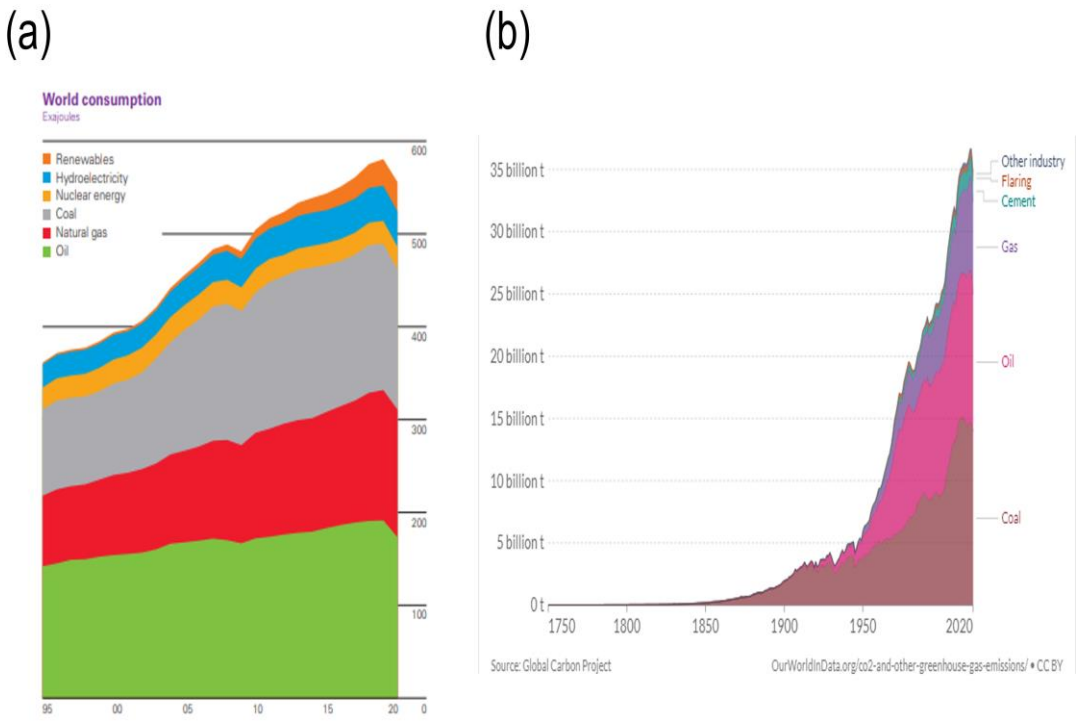

Figure 1.1 a) World energy consumption mix.[2] b) CO_2 emissions by different fuel type.[3]

1.2 Influence of fossil fuel consumption on ecosystem

Since the beginning of time, there exists a balance in nature and this balance is essential for the survival of mankind. However, human-engineered activities can introduce irreversible disorders in our environment. Although, natural disasters may also be the reason for this disorder which may not cause as much harm as human activities do. But human activities are more dangerous to mankind's survival than natural disasters i.e. floods, earthquakes, etc. It all started with the industrial revolution that began in the 18th century and continued playing its demeaning role in environmental destruction. In addition, use of fossil fuels in the transport sector has also bolstered up this rate. Moreover, the power sector is another major source of GHG emissions. Although, by the time, fossil fuels-based systems have acquired developed infrastructure and a highly efficient economy as compared to other energy sources along with dominant socio-economic progress, their impact on climate is catastrophic. Developing economies like China, and India is using coal excessively for their industrial growth and acting as leading environmental pollution actors. Environmental pollutants emitted from fossil energy fuels consumption are presented in the following table. 1.1.

Table. 1.1. Types of environmental pollutant, their sources, and their impacts on human health

Sr No.	Environmental pollutant	Source	Impacts on human health
01	Carbon Monoxide (CO)	i) Incomplete combustion of fossil energy fuels causes emissions of CO	i) Causes diseases like shortness of breath and dizziness
02	Nitrogen Oxides (NO_2, NO)	i)Fossil fuel combustions at very high temperatures, usually above 1300 C, normally occur in automobiles	i) NO_2 can cause respiratory illness ii) Children may get affected badly by alleviated NO_2 levels
03	Sulfur Dioxide (SO_2)	i)SO_2 emissions occur during coal combustions in thermal power plants	i) Causes respiratory illness, chronic lung diseases, alterations in lungs defenses, Asthmatics ii) Plants that are sensitive to SO_2 may get damaged.
04	Particulates Matter (PM_{10}, $PM_{2.5}$)	i)Particulates are emitted into the environment by fossil fuel combustions through industries' outlet chimneys	Causes diseases include i)respiratory ii)cardiovascular iii) damage to lung tissues iv) Premature Death
05	Green House Gases (GHG)	i) SO_2, CO_2, NO_x, CH_4 emissions take place through combustions of coal, gas, and oil	i) GHG are primarily responsible for climatic change and global warming resulting in elevated earth temperature and glaciers melting

1.3 Sustainable development goals (SDGs)

As per the United Nations (UN) mutual agreement, in order to achieve a sustainable development for the betterment of the entire world population, they have signed an agenda in September 2015 to end poverty protect the planet and ensure all people enjoy prosperity and peace, which is known as sustainable development goals or SDGs as shown in Figure 1.2.[4] SDGs are based on the principal of "leaving no one behind" and stress upon the all-inclusive approach for the sustainable development for everyone.

Currently, 1.2 billion people out 7.8 billion of total world population are still deprived from the access to the clean energy for basic life needs including cooking and heating. These people normally obtain energy by burning dry wood or animal dunk which pose great risk to the chronical and respiratory diseases. Therefore, to mitigate the consumption of health hazards for energy purposes, it is also included in the SDGs to ensure clean and affordable energy to everyone on the planet by 2030, known as the 7th goal of the SDGs.

Figure 1.2 Sustainable development goals laid out by UN 2030 agenda.[4]

1.4 Renewable energy: a source of hope to mitigate climate change

Meanwhile, fossil fuels (Coal, Gas and Oil) are used excessively to meet the energy demands of the world, their sources are depleting rapidly fuelling GHG emissions and climate change. Renewable energy has come forth as a source of hope to counter the dilemma of fossil fuels depletion and their catastrophic impact on the ecosystem of the planet earth. Renewable energy source such as solar, wind, hydro, tidal etc. are the inexhaustible sources of energy. However, among them, solar energy has attracted an unprecedented attention of the industrial and scientific community because of the following reasons: i) availability of sunlight and ii) ease of installation.

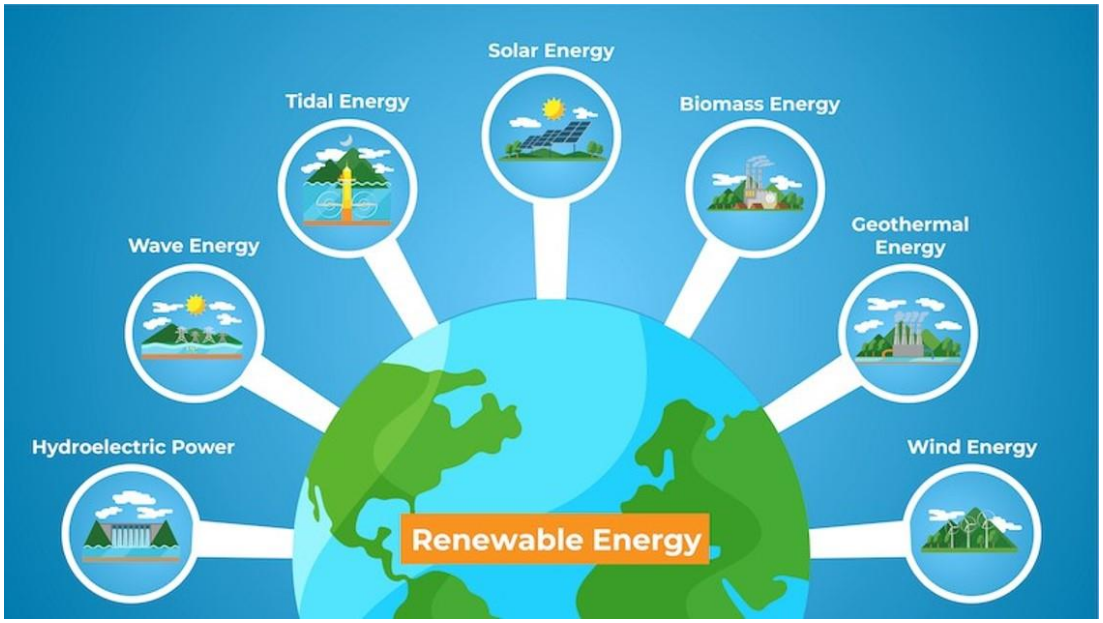

Figure 1.3 Schematic illustration of various renewables and their role to mitigate climate change.[5]

1.5 Evolution of photovoltaic solar cells

After the discovery of photovoltaic effect by Einstein in 1839, researchers started working to develop energy devices that can directly convert sunlight into electricity by using photovoltaic effect. The ground shaking breakthrough was achieved in Bell laboratories in 1950s when they successfully developed silicon based photovoltaic solar cell at commercial level for space applications. These solar cell devices were later known as the Ist generation of the solar photovoltaic. The 1st generation of the photovoltaic solar cells was primarily based on silicon based technology including monocrystalline and polycrystalline solar cells. For quite some time, this technology ruled the research scale. However, there were two major challenges that restricted large scale application of this technology: i) highly energy intensive processes for

silicon extraction and ii) power to weight ratio of silicon based solar cells. To overcome these challenges, further progress was made to develop light weight photovoltaic solar cells such as cadmium telluride (CdTe) and copper indium gallium selenide (or sometimes called CIGS) based solar cells were developed, known as the 2nd generation of the photovoltaic solar cells. Although, 2nd generation of photovoltaic solar cells were useful to offer cost competitive solutions, but they were mainly restricted due to their unfriendly environment character and upscaling problems.

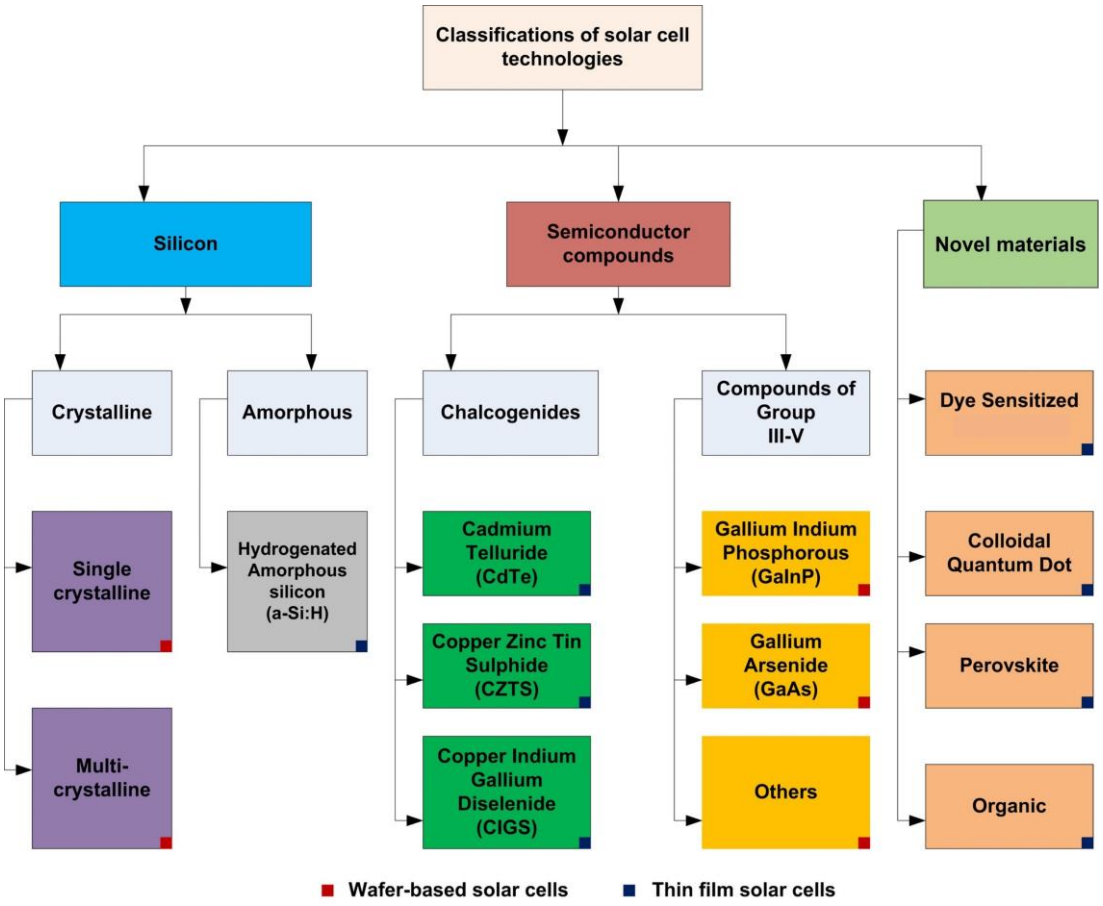

Figure 1.4 Evolution of solar cells along with their different types.[6]

To address all these issues, a 3rd generation of photovoltaic solar cells has evolved for the last three decades. The 3rd generation of the photovoltaic solar cells is fundamentally based on thin film technology offering unprecedented advantages including higher power conversion efficiencies (PCEs), high power to weight ratio, ease of fabrication, low-cost fabrication techniques etc. The leading 3rd generation photovoltaic solar cells technologies includes the following:

- Perovskite solar cells (PSCs)
- Dye-sensitized solar cells (DSSCs)

- Organic/polymer solar cells
- Quantum based solar cells

PSCs have emerged as the most competent type of solar cells for the last decade with an exponential growth in their PCEs from 3.2% in 2009 to 25.8% in 2021 in just 12 years.[7], [8] However, PSCs large scale manufacturing and application is mainly limited due to the lead poisoning and their limited lifetime in ambient environment. These two challenges restrict public acceptance and their manufacturing at industrial scale.

1.6 PSC device construction and working principal

PSCs are primarily constructed in the p-i-n or n-i-p device structure where p denotes hole transport layer, i denotes photoactive or absorber layer and n denotes electron transport layer. Normally, the devices which are constructed using p-i-n configuration are known as inverted solar cells and those which are constructed using n-i-p device architecure are known as normal solar cells. Overall, a PSC device is composed of the following components:

- Transparent conducting oxide (TCO) based electrode
- Electron transport layer (ETL)
- Perovskite based photoactive layer
- Hole transport layer (HTL)
- Noble metal (gold, silver, aluminium, or copper) or carbon based counter electrode

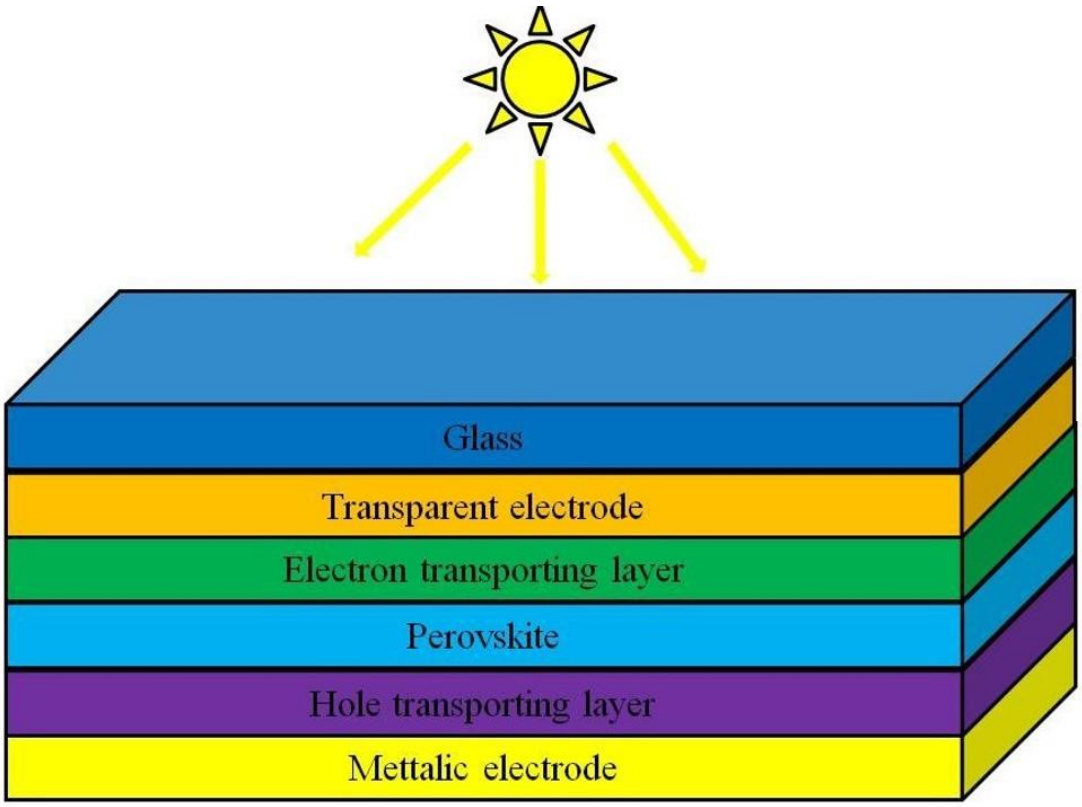

Figure 1.5 Schematic diagram of a standard perovskite solar cell.[9]

Most frequently used TCOs based electrodes include fluorine doped tin oxide (FTO) or indium doped tin oxide (ITO) where charge carriers are collected, and light enters the solar cell device. ETLs are used to extract photogenerated electrons and block holes. Generally, two types of ETLs are used organic or inorganic ETLs based upon the type of the structure of the solar cells. Usually, organic ETLs such as fullerene derivatives are used in inverted PSCs and inorganic ETLs such as titanium oxide or tin oxide are used in normal PSCs. For the photoactive layer based on perovskite structure, methylammonium lead iodide (MAPbI3) based perovskite layer is the most extensively studied photoactive layer for PSCs. However, due to the stability issues and lead poisoning of the MAPbI3, various other photoactive layers have been used in PSCs. HTLs are used to extract photogenerated hole charge carriers and block the electrons. HTLs are also come in different types organic or inorganic. Finally, metals such as gold, silver or aluminium are used as counter electrodes to extract charge carriers out of the PSC device.

In PSC devices, sunlight enters from the TCO electrode's side and is absorbed by the perovskite photoactive layer. As a result, an electron hole pair is generated. These electron hole pairs have very low binding energies. The electron hole pair is dissociated into the electron and hole charge carriers under the influence of ambient

temperature. The electron and hole charge carriers are extracted by the ETL and HTLs, respectively. Then, these charge carriers are finally collected by the TCO based electrodes and metal electrodes depending upon the type of the device structure configuration.

1.7 Challenges of perovskite photoactive layer

The first ever PSC device was constructed using MAPbI3 as photoactive layer with a record PCE of 3.81% [7]. Since then, most of the work was done using MAPbI3 based perovskite layer. However, the MAPbI3 based perovskite photoactive layer has two major intrinsic challenges for their application in PSC. Firstly, the presence of the organic part methylammonium ion restricted their ambient stability due to its volatile nature under ambient environment. The organic part of the traditional perovskite layer interacts with the moisture present in the environment and dissociates into organic halide and metal halides losing the perovskite structure along with its outstanding optoelectronic properties. Secondly, the presence of toxic lead in the MAPbI3 raised many concerns with respect to their application at the large scale. As a result, lead toxicity became one the decisive factor for the sustainable future of PSCs based photovoltaic technology.

1.7.1 Lead toxicity

Naturally, lead (Pb) is found in earth's crust as a component of minerals and rocks. Although, it is not harmful for environment with its natural concentrations. But, for the last 200 years, with the boom in industrial sector, lead applications increased globally. Still, it is widely used in gasoline, paints and pigments, ceramics, metal alloys, car batteries (Lead acid batteries) and solder etc. As a result, anthropogenic lead emissions reached higher levels perturbing natural equilibrium of Pb concentrations. Consequently, new concentration levels degraded air quality badly leaving adverse effects on ambient environment. Thus, various protocols (Montreal, Kyoto etc.) were implemented to gradually reduced health hazard pollutants (Lead, NOx, PM). It is a proven fact that higher concentrations of lead in human body have unhealthy effects. Mostly, lead causes severe diseases i.e., organ damage, blood and heart disease, neural disorder etc. A study done by European Union (EU's) on risk assessment by usage of leaded compounds revealed that children are more susceptible to be affected by lead particles intake through air, water, food etc.[10]. In addition, many studies have been performed which suggest that lead leakage from PSCs can have drastic impact on the ecosystem [11]–[15]. Therefore, while human community

is still struggling to overcome this problem, commercializing lead-based perovskite solar cells will only add fuel to the fire. For this reason, it is indispensable to strive for the ecofriendly perovskite solar devices.

1.8 Problem statement

This work is an endeavour to develop eco-friendly perovskite photoactive layers for the PSC device applications to realize a sustainable future for this exotic solar photovoltaic technology. It is focussed to mitigate lead toxicity through applying compositional engineering and by partially replacing lead in traditionally used MAPbI3 perovskite layer with an element having similar ionic radii, tin (Sn), to develop mixed tin-lead (Sn-Pb) perovskite films.

1.9 Objectives

The main goals of this research work are to develop ecofriendly perovskite films for applications in efficient PSC devices:

- To synthesize ecofriendly perovskite films by compositional engineering of the halide-based precursors
- To perform characterization of the fabricated perovskite films to optimize optoelectronic properties
- To investigate suitability of as such fabricated perovskite films in PSCs

1.10 Scope of the work

This research domain is selected in accordance with the following national needs to achieve autonomy for satisfying energy requirements:

1.10.1 Energy security

Modern day economy is highly dependent on uninterruptable supply of energy. Because of this reason, developed world countries have focused to establish technologies sufficient enough to provide secure and reliable means of energy. As a result, global trends are shifting to harvest energy from renewables' that are abundant and clean. Currently, Pakistan is relying upon fossil fuels (Oil, Gas and Coal) to meet national energy needs, comprising more than 80% of its energy mix [16]. Fossil fuels usage is discouraged for their environment unfriendly nature and limited resources. Since Pakistan lacks relevant technological knowledge to consume its own fossil fuel resources, therefore, it puts extra burden on economy to import expensive fuels from other countries. Moreover, it also endangers sovereignty and strategic position of the

country in the region. Thus, national security is directly related to the self-dependent energy supply.

1.10.2 Technology transfer and development of autonomous photovoltaic industry

Sun is one of the unlimited sources of energy which shines upon us for the whole year. As time pass by, technologies have been developed to employ this source to meet energy demands. At the present time, silicon-based technology is dominating photovoltaic industry. Although, it is commissioned all over the world and successfully gained public trust, however, it is less efficient with high capital costs than competing technologies. Our photovoltaic industry is completely based on imports from countries like China, Germany, and Japan etc. Not being able to fabricate solar systems at home, add import costs as well, raising energy per unit price. Consequently, domestic, and industrial user suffers. Third generation photovoltaic technology is recommended over existing silicon-based technology due to high efficiency and low cost. This research work will be helping in transfer of technology and improvement of energy economy. Furthermore, it will be producing thoughtful and skilled manpower to foresee coming challenges to establish photovoltaic industry in Pakistan.

1.11 Areas of application

1.11.1 Photovoltaic devices

Lead less or lead free (eco-friendly) perovskite solar cells will revolutionize photovoltaic industry since they promise high efficiency and low cost. As a result, we will be able to harness more energy from Sun exerting less resources. Consequently, energy per unit price will decrease which will foster economies uplifting living standards while overcoming poverty challenges.

1.11.2 Optoelectronic devices

Perovskites have demonstrated exceptional potential for applications in optoelectronic devices (LEDs, diodes, and laser diodes etc.). However, these devices are also facing similar problems of lead toxicity same like in photovoltaic domain. This research work will also benefit electronic industry to fully utilize perovskites potential without being concerned of lead usage repercussions.

Summary

This chapter develops the context for the need of solar photovoltaic technology highlighting the current crises of climate change originating from the excessive use of fossil fuels as the available source of energy. Moreover, it also discuses the impact of fossil fuels consumption on the entire ecosystem and particularly on human health. Then, it states the role of renewable energy to mitigate climatic change effects and the bright future of solar photovoltaic technology as a leader to bring this change. Further, it states the different generations of the photovoltaic solar cells and the progress of PSC devices including their challenges. Afterwards, it discusses the problem statement and objectives of this work including scope of the work and its consequential impacts in the longer period.

References

[1] L. (International E. A. Cozzi and T. (International E. A. Gould, "World Energy Outlook 2021," pp. 1–386, 2021, [Online]. Available: www.iea.org/weo.

[2] British Petroleum Company, "Statistical Review of World Energy 2021," BP Energy outlook 2021, vol. 70, pp. 8–20, 2021, [Online]. Available: https://www.bp.com/en/global/corporate/energy-economics/statistical-review-of-world-energy.html.

[3] https://ourworldindata.org/emissions-by-fuel (accessed Jun. 05, 2022).

[4] "Envision2030: 17 goals to transform the world for persons with disabilities United Nations Enable."

[5] "The Importance of using Renewable energy in the efforts to curb climate change | by Save the earth | Medium."

[6] T. Ibn-Mohammed et al., "Perovskite solar cells: An integrated hybrid lifecycle assessment and review in comparison with other photovoltaic technologies," Renew. Sustain. Energy Rev., vol. 80, pp. 1321–1344, Dec. 2017, doi: 10.1016/J.RSER.2017.05.095.

[7] A. Kojima, K. Teshima, Y. Shirai, and T. Miyasaka, "Organometal halide perovskites as visible-light sensitizers for photovoltaic cells," J. Am. Chem. Soc., vol. 131, no. 17, pp. 6050–6051, 2009, doi: 10.1021/ja809598r.

[8] H. Min et al., "Perovskite solar cells with atomically coherent interlayers on SnO2 electrodes," Nature, vol. 598, no. 7881, pp. 444–450, 2021, doi: 10.1038/s41586-021-03964-8.

[9] N. G. Park, "Perovskite solar cells," RSC Energy Environ. Ser., vol. 2014-Janua, no. 11, pp. 242–257, 2014, doi: 10.5757/vacmag.1.4.10.

[10] A. Tukker, H. Buist, L. van Oers, and E. van der Voet, "Risks to health and environment of the use of lead in products in the EU," Resour. Conserv. Recycl., vol. 49, no. 2, pp. 89–109, Dec. 2006, doi: 10.1016/J.RESCONREC.2006.03.005.

[11] B. Conings, A. Babayigit, and H. G. Boyen, "Fire safety of lead halide perovskite photovoltaics," ACS Energy Lett., vol. 4, no. 4, pp. 873–878, 2019, doi: 10.1021/acsenergylett.9b00546.

[12] G. Schileo and G. Grancini, "Lead or no lead? Availability, toxicity, sustainability and environmental impact of lead-free perovskite solar cells," J. Mater. Chem. C, vol. 9, no. 1, pp. 67–76, 2021, doi: 10.1039/d0tc04552g.

[13] I. R. Benmessaoud et al., "Health hazards of methylammonium lead iodide based perovskites: Cytotoxicity studies," Toxicol. Res. (Camb)., vol. 5, no. 2, pp. 407–419, 2016, doi: 10.1039/c5tx00303b.

[14] A. Babayigit, A. Ethirajan, M. Muller, and B. Conings, "Toxicity of organometal halide perovskite solar cells," Nat. Publ. Gr., vol. 15, no. 3, pp. 247–251, 2016, doi: 10.1038/nmat4572.

[15] B. Hailegnaw, S. Kirmayer, E. Edri, G. Hodes, and D. Cahen, "Rain on methylammonium lead iodide based perovskites: Possible environmental effects of perovskite solar cells," J. Phys. Chem. Lett., vol. 6, no. 9, pp. 1543–1547, 2015, doi: 10.1021/acs.jpclett.5b00504.

[16] E. Y. Book, "Primary energy mix," pp. 203–221, 2012.

Chapter 2 Literature Review of Environment Friendly PSCs

Lead halide perovskite solar cells (LH-PSCs) have received unprecedented attention during the last decade due to their superior photoelectric properties and low-cost solution-processable fabrication techniques. Owing to the intensive research efforts, LH-PSCs power conversion efficiency (PCE) values have soared from 3.2% to 25.8% in a few years.[1], [2] As they are racing towards commercialization, lead toxicity is a major obstacle standing in the way. Lead is a heavy metal that has severe health and environmental concerns.[3] Lead poisoning due to the large-scale production of LH-PSCs will have serious repercussions on the entire ecosystem.[4]–[7] Therefore, it is necessitous to completely remove lead from LH-PSCs to gain public acceptance and a sustainable future.

To mitigate lead toxicity, generally, two strategies have been reported in the literature: i) preventing exposure of lead into the environment using encapsulation or lead sequestration techniques[8]–[12]; ii) the complete removal of lead from PSCs. In this regard, several theoretical studies and experimental investigations have been performed to identify potential lead substituents for PSC applications. For example, tin, germanium, bismuth, silver and, alkaline earth metals (magnesium, calcium, barium, and strontium).[13-30] Despite showing great potential to replace lead from PSCs, the substitution of these elements often resulted in a decrease in efficiency.[30]–[32] Interestingly, tin halide based perovskites (THPs) have evolved as front runners among lead-free perovskites due to similar ionic radii of tin, its environmentally benign character and, outstanding optoelectronic properties such as high absorption coefficients, low optical bandgaps (1.2-1.4 eV), high charge carrier mobilities (~585 $cm^2\ V^{-1}s^{-1}$) and low-exciton binding energies (< 20 meV).[33]–[37]

Meanwhile, inspired by the great potential of THPs as a lead-free perovskite absorber, researchers have started working earlier on developing tin halide-based PSCs (TH-PSCs).[1], [13], [36], [38] Initial experimental works on TH-PSCs have suggested that THPs are extremely unstable in ambient conditions, mainly, due to the facile tin oxidation and poor film morphology. Later, it was discovered that tin doping conditions play a significant role to retard tin oxidation.[39] Resultantly, tin halides including tin fluoride (SnF_2), tin iodide (SnI_2), tin bromide ($SnBr_2$), tin chloride

($SnCl_2$) and metallic tin powder based additives were extensively used as tin compensator.[40] However, their excessive use was restricted in TH-PSCs because excess doping of tin halides produced phase segregation which deteriorated tin-based perovskite film morphology.[37], [38] Therefore, significant efforts were made to find suitable additives that can simultaneously inhibit tin oxidation and regulate the fast crystallization of THPs. In this regard, bifunctional additives (BAs) containing different functional groups have been frequently used in TH-PSCs. Consequently, TH-PSCs performance has progressed significantly, approaching 15% PCE milestone, although still lagging to their predecessors LH-PSCs.[2], [41]

2.1 Factors responsible for the performance degradation of TH-PSCs

In this section, we discuss systematically the phenomena that cause the deterioration of TH-PSCs efficiency and stability, starting from summarizing reports available on origins of tin oxidation and concluding on the poor morphology of THPs.

2.1.1 Origins of tin oxidation

Tin (Sn) and lead (Pb), both elements belonging to IVA group of the periodic table, possess electronic configurations $[Kr]4d^{10}\mathbf{5s^2 5p^2}$ and $[Xe]4f^{14}5d^{10}\mathbf{6s^2 6p^2}$, respectively as shown in Figure 2.1 a. IVA group elements are known to have variable oxidation states, +2 and +4 as the most frequent. Notably, Sn^{2+} is desired for optoelectronic applications due to its suitability to form organic/inorganic hybrid perovskite structures as $ASnX_3$ where A= monovalent cation i.e., MA^+ (methylammonium ion) , FA^+ (formamidinium ion) or Cs^+ (caesium ion) and X= monovalent anion e.g. I^- (iodide ion), Br^- (bromide ion) or Cl^- (chloride ion). It is noted that the +2 oxidation state is more stable for elements at the bottom of the IVA group. Even though tin exists in the divalent state (Sn^{2+}), it is more stable in the tetravalent state (Sn^{4+}). Conversely, lead is stable in the Pb^{2+} state due to the prominent inert pair effect resulting from higher relativistic contraction. This relativistic contraction stems from the higher effective nuclear charge experienced by ns^2 valence electrons of Pb atoms as compared to Sn atoms, which stabilizes the Pb^{2+} oxidation state under standard conditions. This peculiar nature of atomic tin remains a fundamental source of tin oxidation and high hole conductivity in TH-PSCs.[35], [42] Initially, caesium tin iodide ($CsSnI_3$) was used as hole transport material in dye-sensitized solar cells due to its high hole mobility (585 $cm^2\ V^{-1}\ s^{-1}$).[43] Thus, tin does not enjoy perks of having a stable +2 oxidation state and, hence, attaining an efficient and stable lead-free TH-PSCs has remained a problem for researchers.

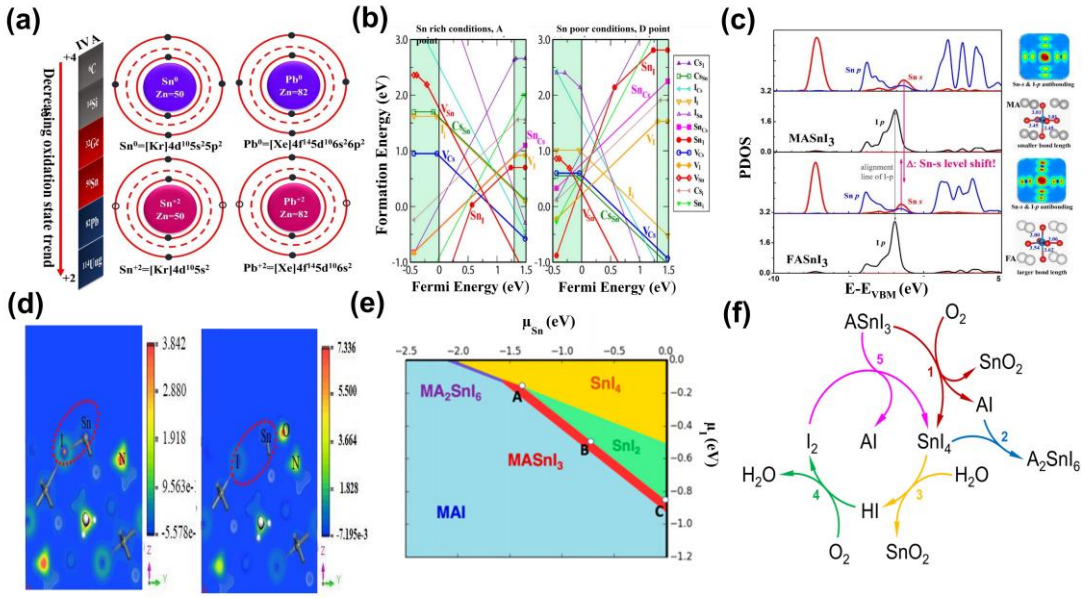

Figure 2.1 (a) Oxidation state trend in the down part of group IVA and dot structure of tin and lead. b) Formation energies of tin and cesium vacancies (V_{Sn} and V_{Cs}) as a function of tin doping conditions.[39] c) Partial density of states (PDOS) of tin and iodine, bond lengths, and partial charge density around valence band maximum $FASnI_3$ (Formidinium tin iodide) and $MASnI_3$ (Methylammonium tin iodide).[44] d) Electron density of (i) a (001) clean surface and (ii) O_2 adsorbed on the surface. e) Phase diagram of $MASnI_3$.[46] f) THPs cyclic degradation process in atmospheric conditions.[47]

Indeed, it is inevitable that tin perovskites will undergo oxidation in the ambient environment, which will result in loss of optoelectronic properties. For this reason, it is necessary to find optimum growth conditions for stabilizing Sn^{2+} to preserve the perovskite structure required for optoelectronic applications. In this regard, a seminal work was reported by Xu *et al.*, where they theoretically explored the role of synthesis conditions on the nature of $CsSnI_3$ material. They found that cesium and tin vacancies (V_{Cs} and V_{Sn}, respectively) have low formation energies under poor tin doping conditions, as shown in Figure 2.1 b. As a result, tin perovskites showed high concentrations of acceptor defects resulting in enhanced hole mobility of the material. Whereas, under moderate tin doping, the same material showed a decrease in the concentration of acceptor defects, which subsequently reduced the hole concentrations, making it suitable for photovoltaic application.[39] In another work, Shi *et al.* studied the effect of organic cation (MA^+ or FA^+) substitution at A-site on tin vacancies in THPs. They found that formamidinium based tin perovskite showed

higher formation energies for tin vacancies as compared to $MASnI_3$-based perovskites due to weak antibonding interaction between Sn-s and I-p, stemming from the large size of the formamidinium cation as seen in Figure 2.2 c.[44] Later, Leijtens *et al,* studied oxidation pathways of pure tin- and mixed lead-tin based perovskites and found that latter showed higher strength against oxidation. Moreover, they also found that pure $ASnI_3$ ($A = MA^+$, FA^+, or Cs^+) dissociated into SnO_2, SnI_4, and organic halide (reaction I). In contrast, lead-tin based perovskites were deteriorated through a different rout. Surprisingly, the formation of SnI_4 was suppressed and $ASn_{0.5}Pb_{0.5}I_3$ dissociated into AI, SnO_2, PbO, and I_2 (reaction II), which made lead-tin perovskites more robust in ambient conditions [48].

$$2ASnI_3 + O_2 \rightarrow 2AI + SnO_2 + SnI_4 \quad \text{(I)}$$

$$2APb_{0.5}Sn_{0.5}I_3 + O_2 \rightarrow 2AI + SnO_2 + PbO + SnI_4 \quad \text{(II)}$$

Another report highlighting the effects of different environments (O_2, H_2O, and N_2) on THPs by Xie *et al,*[45] stated that $MASnI_3$ was more stable under N_2 environment than O_2 and H_2O. They found that the adsorbed molecules of O_2 and H_2O on the perovskite surface attacked Sn---I bond and formed new Sn---O and H---I bonds, respectively, as shown in Figure 2.3 d.

It is believed that tin oxidation of tin based perovskite films start from surface to the bulk[49], [50]; however, a comprehensive computational study was performed by Ricciarelli *et al.* showing that of $Sn^{2+} \rightarrow Sn^{4+}$ oxidation was energetically more favorable at the surface as compared to the bulk, due to the presence of grain boundaries and uncoordinated tin atoms acting as electron traps assisting in lattice degradation.[51] In another work, Meggiolaro *et al.* reported role of V_{Sn} emanating from nonstoichiometric ratios of Sn and I atoms on lattice degradation of $MASnI_3$ perovskites. They found that V_{Sn} created iodine rich environment which subsequently assisted Sn^{2+}/Sn^{4+} oxidation, as seen in Figure 2.4 e.[46] Recently, Lanzetta *et al,* investigated tin perovskites degradation through iodine-assisted oxidation in ambient environment. They reported that oxidized SnI_4 impurities present in tin-based perovskite films initiate a cyclic degradation process by reacting with H_2O and O_2, as shown in Figure 2.5 f. As a result, I_2 further oxidize SnI_2 into SnI_4 and the cycle continued to degrade tin-based perovskite films.[47]

2.1.2 THPs poor morphology

Stabilizing tin halide-based perovskite film morphology is pivotal towards achieving high-performance lead-free TH-PSCs. Large grains, smooth and pinhole-free films, and complete substrate coverage promote crystallinity, facilitate charge transportation and block shunting paths between electrodes to avoid short-circuiting of the devices. PbI_2 (lead iodide) and MAI (methylammonium iodide) form a yellowish intermediate adduct with DMSO (dimethyl sulfoxide) and DMF (N,N-dimethylformamide) i.e., MAI: DMSO/DMF: PbI_2 after being spin-coated on glass-substrates (Figure 2.2 a). Upon thermal treatment at elevated temperatures (≥100 ^{o}C), the residual solvent evaporates and black phase perovskite is formed. On the other hand, the chemical reaction between MAI and SnI_2 is much faster than in the case of lead iodide.[52] For this reason, tin-based perovskite film changes its color from transparent yellow to reddish brown even at room temperature, indicating fast crystallization (Figure 2.2 b).[53] Liao *et al*,[54] reported morphology issues of tin-based perovskite films on PEDOT:PSS (poly(3,4-ethylenedioxythiophene):poly(styrenesulfonate). They found that that They found that flower like structures along with many pinholes were formed when $FASnI_3$ films were deposited on PEDOT:PSS leading to the short-circuiting of the devices, as seen in Figure 2.2 c. Moreover, it has also been observed that excessive use of tin halides as tin compensators induce phase segregation destroying tin perovskite film morphology as shown in Figure 2.2 d-f.[37], [38], [55]

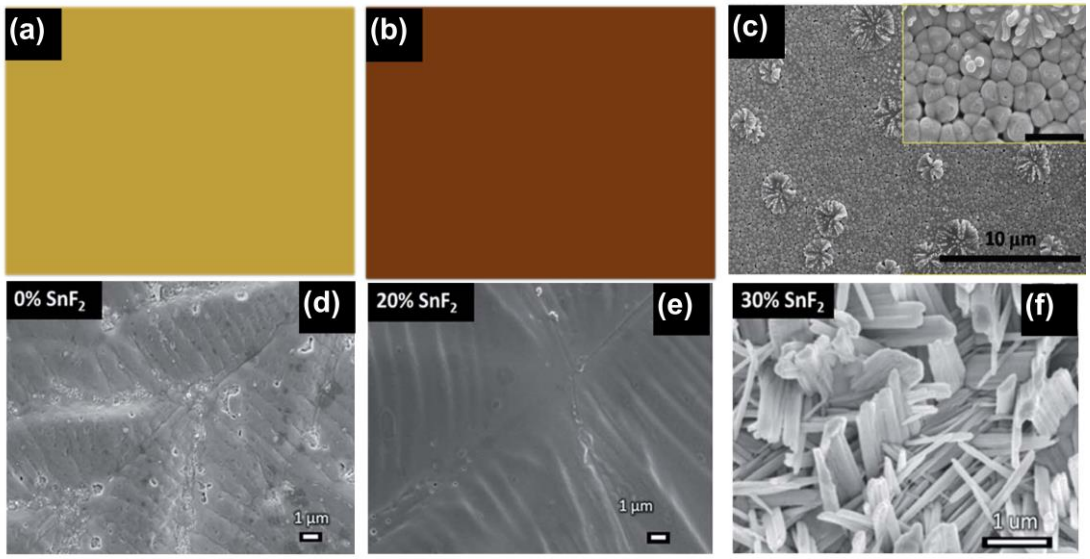

Figure 2.2 a) Image of MAI:DMSO/DMF:PbI_2 non-annealed perovskite film.[1] b) Image of MAI:DMSO/DMF:SnI_2 non-annealed perovskite film.[13] c) Scanning electron microscopy (SEM) image of $FASnI_3$ perovskite on the top of PEDOT:PSS

film.[54] d-f) SEM images of $FASnI_3$ doped with 0 mol% SnF_2, 20 mol% SnF_2 and 30 mol% SnF_2 respectively.[37]

2.2 Conventional strategy to provide excess tin source as Sn^{+2} compensator in TH-PSCs

2.2.1 $CsSnX_3$ (X=I, Cl and Br) based TH-PSCs

$CsSnI_3$ is notorious for showing polymorphism (cubic, tetragonal and orthorhombic). [56], [57] Whereas, for photovoltaic applications, the βγ-phase of $CsSnI_3$ is needed. Initially, Chen *et al.* published a report on $CsSnI_3$ used as absorber layer in schotkey-junction solar cells with a very low efficiency (up to 0.9%), due to the high series and low shunt resistances.[58] Later, Kim *et al.* studied the influence of tin halides on stabilizing photoactive phase of $CsSnI_3$ through passivation of tin vacancies. They stated that $SnBr_2$ was most promising additive to stabilize photoactive orthorhombic black phase. Supportingly, density-functional theory (DFT) calculations showed high formation energies of photo-inactive phase (Y-$CsSnI_3$) upon $SnBr_2$-doping. Consequently, $CsSnI_3$ TH-PSCs showed a PCE of 4.3%.[59] Inspired by the discovery of moderate tin doping conditions during tin based perovskite material synthesis,[39] Kumar *et al. used* SnF_2 as additional tin source to suppress the formation of Sn^{2+} vacancies. SnF_2-$CsSnI_3$ films showed superior electronic properties than pristine perovskite films. The addition of SnF_2 reduced hole carrier density from 10^{19} cm^{-3} to 10^{17} cm^{-3} (Figure 2.3 a). As a result, TH-PSCs showed PCE values up to 2.02% **(**Figure 2.3 b).[38] Marshall *et al*,[60] fabricated all inorganic TH-PSCs in inverted configuration (p-i-n) with cupper iodide (CuI) and fullerene working as charge extraction layers under excess SnI_2, schematic illustration of the TH-PSCs (Figure 2. 6c). During the fabrication, they drop-casted SnI_2 on the perovskite layer surface to inhibit tin oxidation. As a result, these devices showed enhanced PCE up to 2.76%. Gupta *et al.* explored bromine-doped THPs for photovoltaic applications. They used SnF_2 as excess tin source. They found that control TH-PSCs showed open-circuit voltage (V_{oc}) values up to 0.1 V, whereas SnF_2-treated devices exhibited V_{oc} up to 0.4 V and a PCE of 2.17% efficiency (Figure 2.3 d-f).[61] Moghe *et al.* reported vapor deposited SnF_2-doped $CsSnBr_3$ films and demonstrated the fabrication TH-PSCs from thermal evaporation. Although, the overall performance of the devices was poor, but the V_{oc} was improved to 0.44 V and the fill factor (FF) up to 55% upon SnF_2 doping.[62] Marshall *et al.* presented a comparative study to investigate most efficient

tin halide among $SnCl_2$, $SnBr_2$, SnI_2 and SnF_2 for TH-PSCs. They found that $SnCl_2$ was more efficient than others due to two reasons; i) smaller chloride ion size and ii) higher solubility of $SnCl_2$ in traditional solvents (e.g. DMSO, DMF etc.). Consequently, TH-PSCs showed an impressive PCE up to 3.56%. [63]

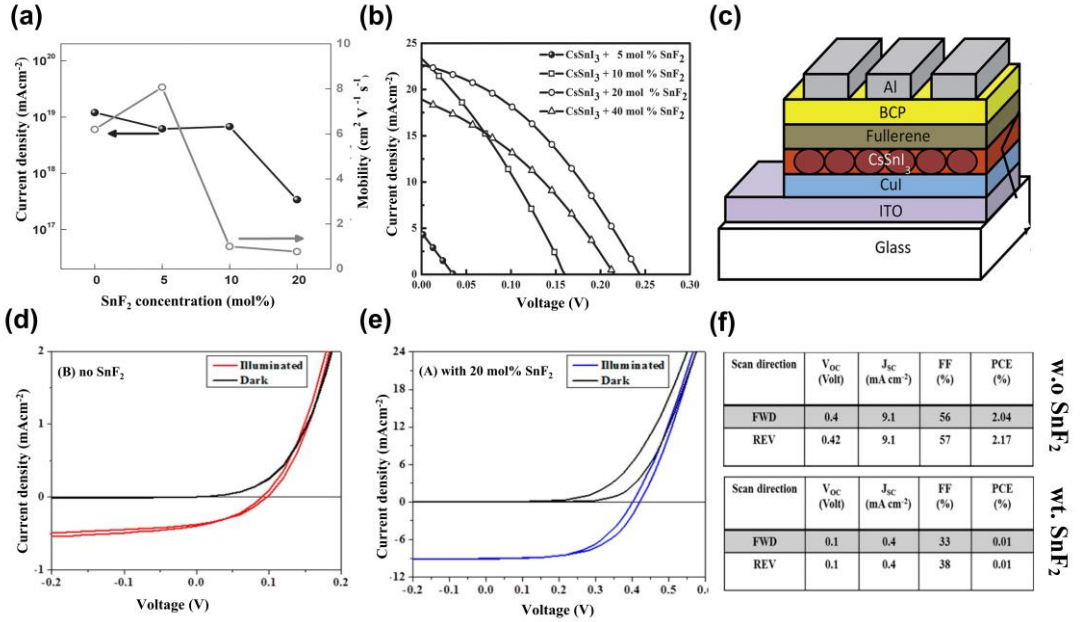

Scan direction	V_{OC} (Volt)	J_{SC} (mA cm^{-2})	FF (%)	PCE (%)
FWD	0.4	9.1	56	2.04
REV	0.42	9.1	57	2.17

w.o SnF_2

Scan direction	V_{OC} (Volt)	J_{SC} (mA cm^{-2})	FF (%)	PCE (%)
FWD	0.1	0.4	33	0.01
REV	0.1	0.4	38	0.01

wt. SnF_2

Figure 2.3 a) Influence of SnF_2 doping on mobility and charge carrier density of $CsSnI_3$ perovskite films. b) J-V curves of $CsSnI_3$-based TH-PSCs with different SnF_2 doping concentrations.[38] c) Schematic illustration of $CsSnI_3$ inverted TH-PSCs.[60] d) and e) J-V curves of control and 20 mol% SnF_2-$CsSnBr_3$ TH-PSCs, respectively. f) Photovoltaic parameters of control and 20 mol% SnF_2-$CsSnBr_3$ TH-PSCs.[61]

2.2.2 $MASnX_3$ (X=I, Cl and Br) based TH-PSCs

Initial reports on $MASnI_3$ based TPSCs fabrication without any additive are dated back to the year 2014, when Noel et. al demonstrated TH-PSCs with promising efficiency above 6% (Figure 2.4 a). However, those devices were very unstable and quickly degraded after being in contact with ambient environment.[13] Just few weeks later, Hao *et al*,[36] applied halide engineering to exploit optoelectronic properties of $MASnI_3$ by changing the bromine concentration and achieved a band gap range from 1.3 eV to 2.15 eV(Figure 2.7 b). Although they were successful to achieve 5.23% PCE with pristine MASnI3, the stability was still remained major challenge.

Another report available without any additive was from Yu *et al.* when they fabricated $MASnI_3$ based TH-PSCs in inverted configuration through hybrid thermal evaporation and reported high coverage ratio with good stoichiometry of $MASnI_3$ perovskite films. They achieved a V_{oc} of 0.494 V, shortcircuit-current density (J_{sc}) of 12.1 mAcm^{-2} with

an overall 1.7% efficiency.[64] Later, Hao *et al.* maneuvered solvent engineering and exploited SnI_2:DMSO adduct as intermediate phase to slow down fast crystallization and obtained pinhole-free and uniform tin-based perovskite films. They used 20 mol% SnF_2 to inhibit Sn^{4+} doping and obtained a J_{sc} of 21 $mAcm^{-2}$ and 3.15% PCE.[53] Kim *et al.* reported $MASnI_3$ based TH-PSCs using SnF_2 as excess tin source and obtained 2.33% efficiency.[65] Handa *et al*,[66] reported effect of SnF_2 doping on optoelectronic properties of $MASnI_3$-based perovskites. They found that SnF_2 as excess tin source stabilized optical bandgap of tin perovskites. Whereas controlled perovskite films without SnF_2 showed an increase in the bandgap due to uncontrolled hole doping (Figure 2.4 c-d). As a result, SnF_2-$MASnI_3$ based TH-PSCs showed a PCE of 1.94%.

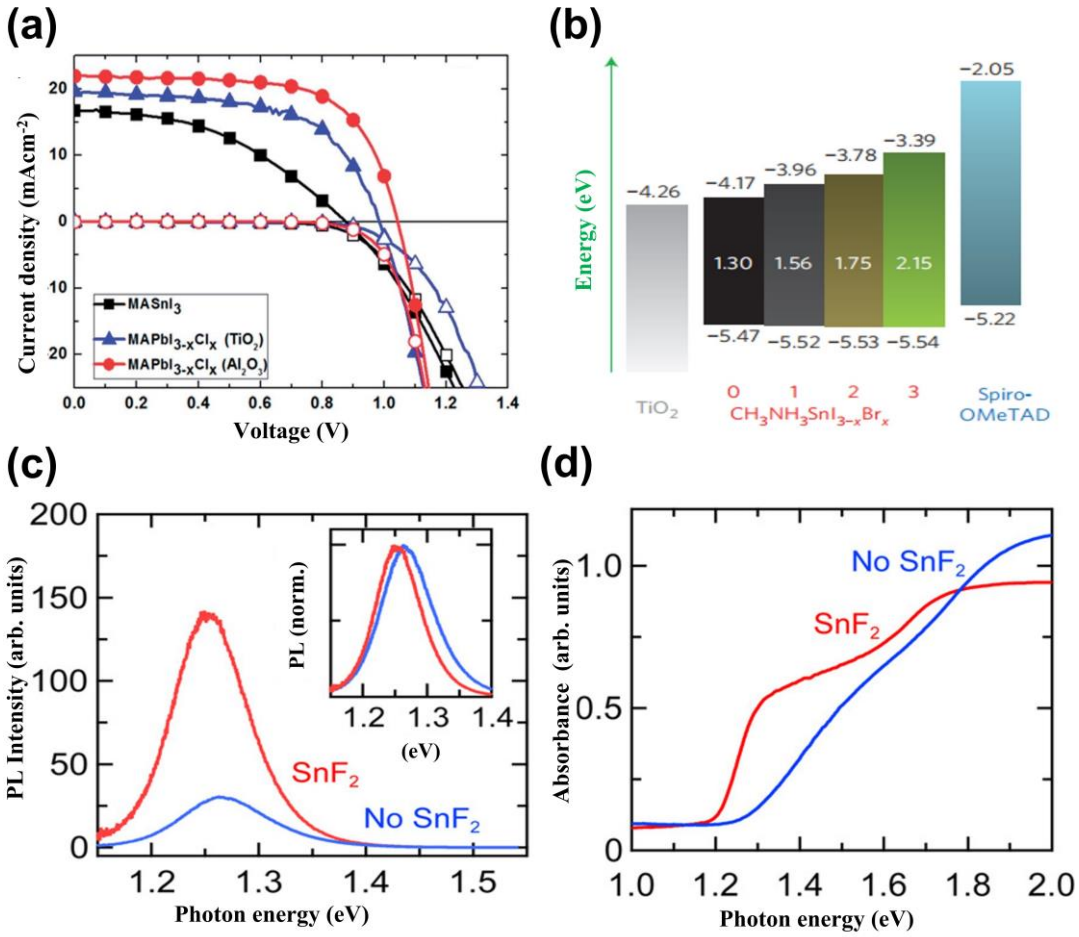

Figure 2.4 a) J-V curves of TH-PSCs and LH-PSCs on TiO_2 and Al_2O_3.[13] b) Influence of halide engineering on optical bandgap of $MASn(I_{1-x}Br_x)_3$.[36] c) and d) Photoluminescence (PL) emission and absorption spectra of $MASnI_3$ perovskite films without and with SnF_2, respectively.[66]

2.2.3 $FASnX_3$ (X=I, Cl and Br) based TH-PSCs

$FASnI_3$ based perovskites are thermally more stable than $MASnI_3$ based perovskites due to the hydrogen bonding of FA^+ with the inorganic octahedra cage (MX_6) [44], [67]. Inspired from high thermal stability and lower bandgap than $MAPbI_3$ (1.47 eV),[68] Koh *et al.* studied $FASnI_3$ based perovskites as photoactive layers having a bandgap of 1.41 eV for photovoltaic applications. X-ray diffraction (XRD) results showed that pure $FASnI_3$ perovskites adopted orthorhombic crystal structure with peculiar unit cell dimensions (a=6.3096, b=8.9298 and c=9.0622) and remained under different annealing temperature (100 ^oC, 150 ^oC, and 200 ^oC), (Figure 2.5 a). To prevent tin oxidation, they used SnF_2, which improved the PCE of TH-PSCs up to 2.1% (Figure 2.5 b and c).[37]

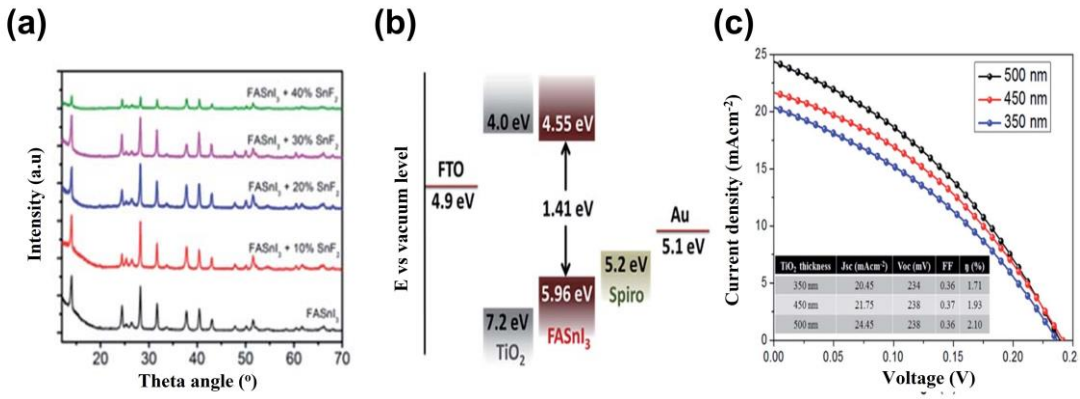

Figure 2.5 a) XRD patterns of SnF_2 doped $FASnI_3$ perovskite films. b) The energy band diagram of valence band maximum (VBM) and conduction band maximum (CBM) of FASnI3, TiO_2, Spiro-OMeTAD and gold electrodes. c) J-V curves of SnF_2-$FASnI_3$ TH-PSCs with different TiO_2 layer thickness.[37]

2.2.4 Mixed-cation mixed-halide TH-PSCs

Mixed-cation mixed-halide TH-PSCs offer peculiar characteristics in comparison with non-mixed cation TH-PSCs, mainly due to better energy band alignment with charge transport layers resulting in good charge transport properties, high V_{oc} and lower hole charge carrier densities, indicating importance of the compositional engineering to obtain high performance TH-PSCs. Sabba *et al.* studied the influence of the bromine substitution in $CsSnI_3$ perovskites. They observed a significant decrease in the background charge carrier density when bromine concentration was gradually increased, decreasing hole carrier density from ~10^{18} for $CsSnI_3$ to ~10^{15} for $CsSnIBr_2$. Similarly, the optical bandgap of the films gradually increased on bromine doping

showing increase in V_{oc} and a decrease in J_{sc} with a PCE of 1.76% (Figure 2.6 a-b), respectively.[69] Zhao *et al.* reported mixed cation $FA_{0.75}MA_{0.25}SnI_3$ perovskite composition as photoactive layer and obtained an efficiency equal to 8.12% due to high V_{oc} (0.61 V) using 10 mol% SnF_2 as Sn^{2+} compensator (Figure 2.6 c).[70] Later, Liu *et al*,[71] explored A-site compositional engineering of $FASnI_3$ perovskite system with SnF_2 as excess tin source. Moreover, they also studied the effect of different antisolvents *i.e.*, chlorobenzene (CB), toluene (TL), and diethyl ether (DE) on film morphology and charge carrier transport. Among them, CB was found as the most efficient antisolvent to obtain uniform and smooth perovskite films (Figure 2.6 d). Resultantly, the PCE of TH-PSCs surpassed 9% (Figure 2.6 e). Later, Li *et al*. reported large area (>20 cm^2) $MA_{0.75}FA_{0.25}SnI_3$-based TH-PSCs using of SnF_2 as additive. They used gas-pump treatment to control tin perovskite films crystallization kinetics instead of typically used anti-solvent washing method. They found that phase segregation induced by SnF_2 disappeared when pressure reached 1500 Pa. As a result, they obtained pinhole-free and uniform perovskite films reaching a PCE of 1.85% (Figure 2.6 f).[72]

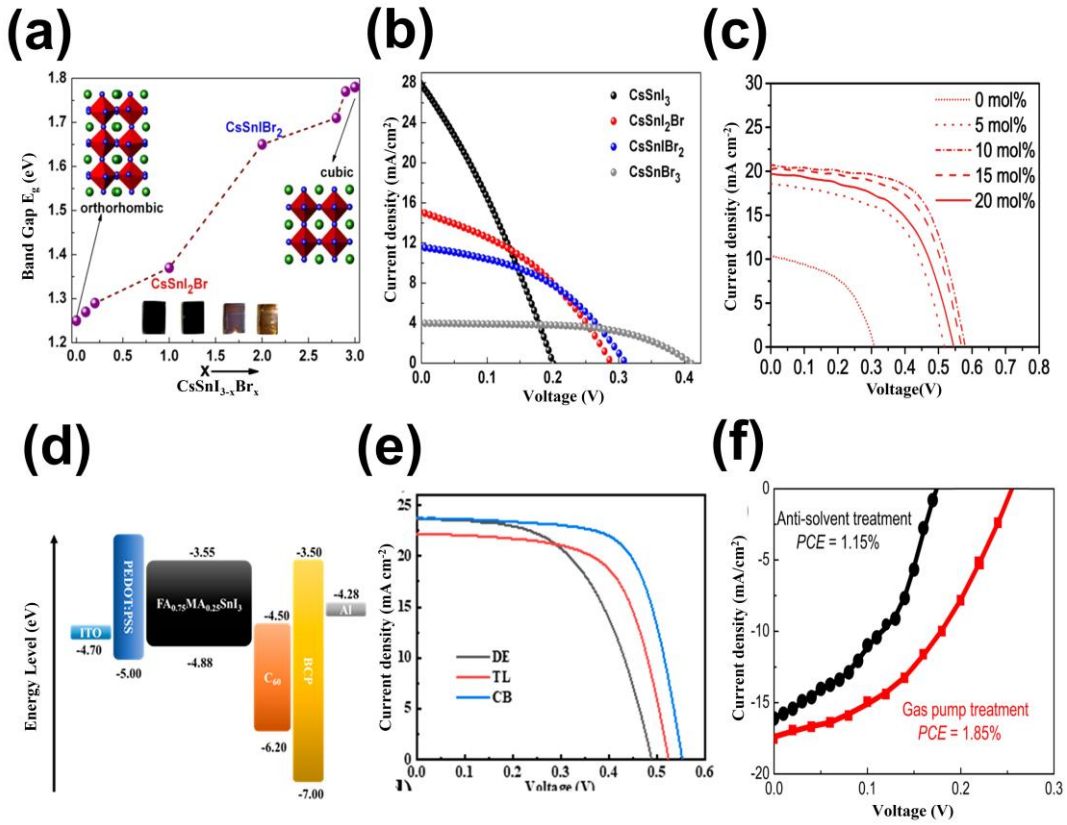

Figure 2.6 a) The bandgap variation of $CsSnI_3$ on bromine-doping. b) J-V curves of bromine-doped $CsSnI_3$ TH-PSCs.[69] c) J-V curves of mixed cation $FA_{0.75}MA_{0.25}SnI_3$

based TH-PSCs with different concentrations of SnF_2.[70] d) Energy band diagram of $FA_{0.75}MA_{0.25}SnI_3$ perovskite, electron and hole transport layers and counter electrodes. e) J-V curves of $FA_{0.75}MA_{0.25}SnI_3$ based TH-PSCs with DE, CB and TL.[71] f) J-V curves of SnF_2-doped $MA_{0.75}FA_{0.25}SnI_3$ based TH-PSCs with antisolvent treatment and gas pump treatment.[72]

Table 2.1 Summary of TH-PSCs photovoltaic parameters with traditionally used additives i.e., tin halides

Year	Perovskite	Additive	PCE [%]	J_{sc} [$mAcm^{-2}$]	V_{OC} [V]	FF [%]	Ref.
2014	FTO/c-TiO_2/mp-TiO_2/$CsSnI_3$/Spiro-OMeTAD/Au	SnF_2	2.02	22.70	0.24	37	[38]
2015	FTO/c-TiO_2/mp-TiO_2/$FASnI_3$/Spiro-OMeTAD/Au	SnF_2	2.10	24.45	0.238	36	[37]
2015	ITO/CuI/SnI_2/$CsSnI_3$/ ICBA/Al	SnI_2	2.76	12.78	0.50	44	[60]
2015	ITO/PEDOT:PSS/Poly-TPD/$MASnI_3$/C_{60}/BCP/Ag	SnF_2	3.15	21.4	0.32	46	[53]
2015	FTO/c-TiO_2/mpTiO_2/$CsSnIBr_2$/Spiro-OMeTAD/Au	SnF_2	1.76	15.06	0.28	38	[69]
2016	FTO/c-TiO_2/mp-TiO_2/ $CsSnBr_3$/ PTAA/Au	SnF_2	2.1	9.0	0.41	58	[61]
2016	ITO/MoO_3/$CsSnBr_3$/ C_{60}/BCP/Ag	SnF_2	0.55	2.6	0.44	55	[62]
2016	ITO/$CsSnI_3$/$PC_{61}BM$/BCP/Al	$SnCl_2$	3.56	10.4	0.51	69	[63]
2016	ITO/PEDOT:PSS/Poly-TPD/ $MASnI_3$/ C_{60}/BCP/Ag	None	1.7	12.1	0.37	36.6	[64]
2017	FTO/c-TiO_2/mp-TiO_2/ $MASnI_3$/ PTAA/Au	SnF_2	2.33	26	0.23	38.6	[65]

2017	FTO/c-TiO_2/mp-TiO_2/ $MASnI_3$/ PTAA/Au	SnF_2	1.94	26.1	0.25	30	[66]
2017	ITO/PEDOT:PSS/ $MASnI_3$/ C_{60}/BCP/Ag	SnF_2	2.49	13.02	0.46	43	[73]
2017	ITO/PEDOT:PSS/ $FA_{0.75}MA_{0.25}SnI_3$/ C_{60}/BCP/Ag	SnF_2	8.12	21.2	0.61	62.7	[70]
2018	ITO/PEDOT:PSS/ $MA_{0.75}FA_{0.25}SnI_3$/ C_{60}/BCP/Al	SnF_2	9.06	24.3	0.55	67.3	[71]
2018	FTO/c-TiO_2/mp-TiO_2/$CsSnI_3$/ PTAA/Au	$SnX_{2,\ (X=\ F,\ Cl\ and\ Br)}$	4.30	18.5	0.44	52.9	[59]
2019	FTO/c-TiO_2/mp-TiO_2/ $FA_{0.75}MA_{0.25}SnI_3$/ PTAA/Au	SnF_2	1.85	17.4	0.26	42	[72]

2.3 Research progress of Sn-Pb mixed PSCs

Recently, Jung et al. , (2019), have achieved a record efficiency of 23.3% of single-junction lead based organo-inorganic hybrid perovskite solar cells (OIHP) through compositional engineering of the absorber layer $(FAPbI_3)_{0.95}(MAPbI_3)_{0.05}$.[74] Ogomi et al. , (2014), was the first one to conduct experimental study on tin based organometal halide perovskite absorber layer ($MASnI_3$). It was found that tin halide (SnX_2) itself exhibit poor photovoltaic performance due to tin instability in ambient environment (Sn^{+2} get oxidized into Sn^{+4}). However, they managed to achieve PCE of 4.12% and a short circuit current of 20.04 $mAcm^{-2}$ with open circuit voltage of 0.42 V and Fill Factor of 50% through optimizing molar ratios of Pb:Sn (50mol%:50mol%) in the active layer ($MAPb_{0.5}Sn_{0.5}I_3$). Furthermore, a 260 nm red shift was also observed in absorption spectra as compared to pristine $MAPbI_3$ films which showed organic inorganic tin halide PSCs have high absorption coefficients.[76] Later on, H.J Snaith and his group achieved a PCE of 6% of lead free tin based perovskite solar cells fabricated with mesoporous TiO_2 and Spiro-OMeTAD as electron transport layer and hole transport layer, respectively, under one sun illumination and bandgap of $MASnI_3$ was stated 1.23 eV.[13]

From then onwards, researchers kept trying to improve film morphology and the ambient stability issues of the tin by using additives (antioxidants) and changing film deposition parameters to enhance photovoltaic performance of the Lead free Tin based PSCS. But outcomes of these efforts were not much effective. As a result, Germanium (Ge), same group element, was also investigated in detail theoretically and recommended as a potential replacement. However, Krishnamoorthy et al. , (2015), studied $MAGeI_3$ and compared it with other fully inorganic $CsGeI_3$ and $FAGeI_3$ films for photovoltaic applications. Their experimental results showed that $MAGeI_3$ films were quite effective against thermal stability but were more susceptible to air oxidation resulting poor performance than $MASnI_3$ absorber layer devices. Consequently, only 0.2% PCE was recorded with short circuit current 4.0 $mAcm^{-2}$ and open-circuit voltage 0.15 V for $MAGeI_3$ based perovskite solar cells.[77] Following Krishna's work, K. Indira et al., (2018), implemented compositional engineering of halide ions and replaced 10% of iodide with Bromide in $MAGeI_xBr_{(1-x)}$. Consequently, achieving a little improvement in PCE from 0.2% to 0.57% along with slight increase in device stability with $MAGeI_{2.7}Br_{0.3}$ as active layer in planar *p-i-n* architecture using PEDOT: PSS and $PC_{60}BM$ as HTL and ETL, respectively.[78] Meanwhile, other potential substituents were also tested but their performance were not even near to the lead based OIHPs devices. For e.g. $MA_3Bi_2I_9$ (PCE 0.33%) [79], $MA_3Sb_2I_9$ (PCE 2.04%) [80] etc.

Hence, it was realized that complete lead removal will not be helpful since photovoltaic performance of the devices was comprised. As a result, intensive efforts were exerted on binary metal compositions to gradually decrease lead concentrations from OIHPs. To the best of my knowledge. M. G Kanantzidis et al., (2014), pioneered this work and speculated binary metal composites of Pb:Sn with 7.27% PCE, short-circuit current 20.64 $mAcm^{-2}$ and open-circuit voltage 0.584 (Voc). They studied band gap (E_g) as a function of Pb:Sn ratio and found that $MAPb_{0.5}Sn_{0.5}I_3$ exhibited broadest absorption spectra at E_g=1.27eV with maximum J_{sc} 20 $mAcm^{-2}$. In addition, it was also reported that bandgap changes does not follow linear relationship (Vegard's law) upon varying Pb:Sn concentrations between two peaks (1.56 eV $MAPbI_3$ and 1.27 $MASnI_3$).[81] This work opened new doors for researchers to explore binary metal compositions suitable for OIHPs. Later in 2017, Lingang Li and his group reported, Lead-Tin mixed OIHPs demonstrating controlled growth of large grains through one-step solution deposition process by solvent engineering of sec-butyl alcohol with DMSO. As a result, they produced large grain size and compact perovskite active layer devices achieving a maximum PCE of 12.08%. However, the problem still remains and it was higher lead concentration with composition $MASn_{0.25}Pb_{0.75}I_3$ which made them less ecofriendly.[82] Considering these short-comings, Gaurav Kapil et al., 2018, introduced interfacial engineering to demonstrate spike structure strategy between absorber layer and ETL (C_{60}). In this way, they successfully achieved 17.6% efficient devices with configuration (ITO/PEDOT:PSS/$FA_{0.5}MA_{0.5}Sn_{0.5}Pb0_{.5}I_3$/PCBM/$C_{60}$/BCP/Ag).[83]

It has been demonstrated that binary metal cation based OIHPs are promising candidates to reach higher photovoltaic performance. However, lead presence is still problematic as it needs to be reduced up to trace levels while having least impact on the device efficiency. Therefore, it is essential to explore binary or even ternary composites which offer which offer superior photovoltaic properties than lead based PSCs.

Flow Chart

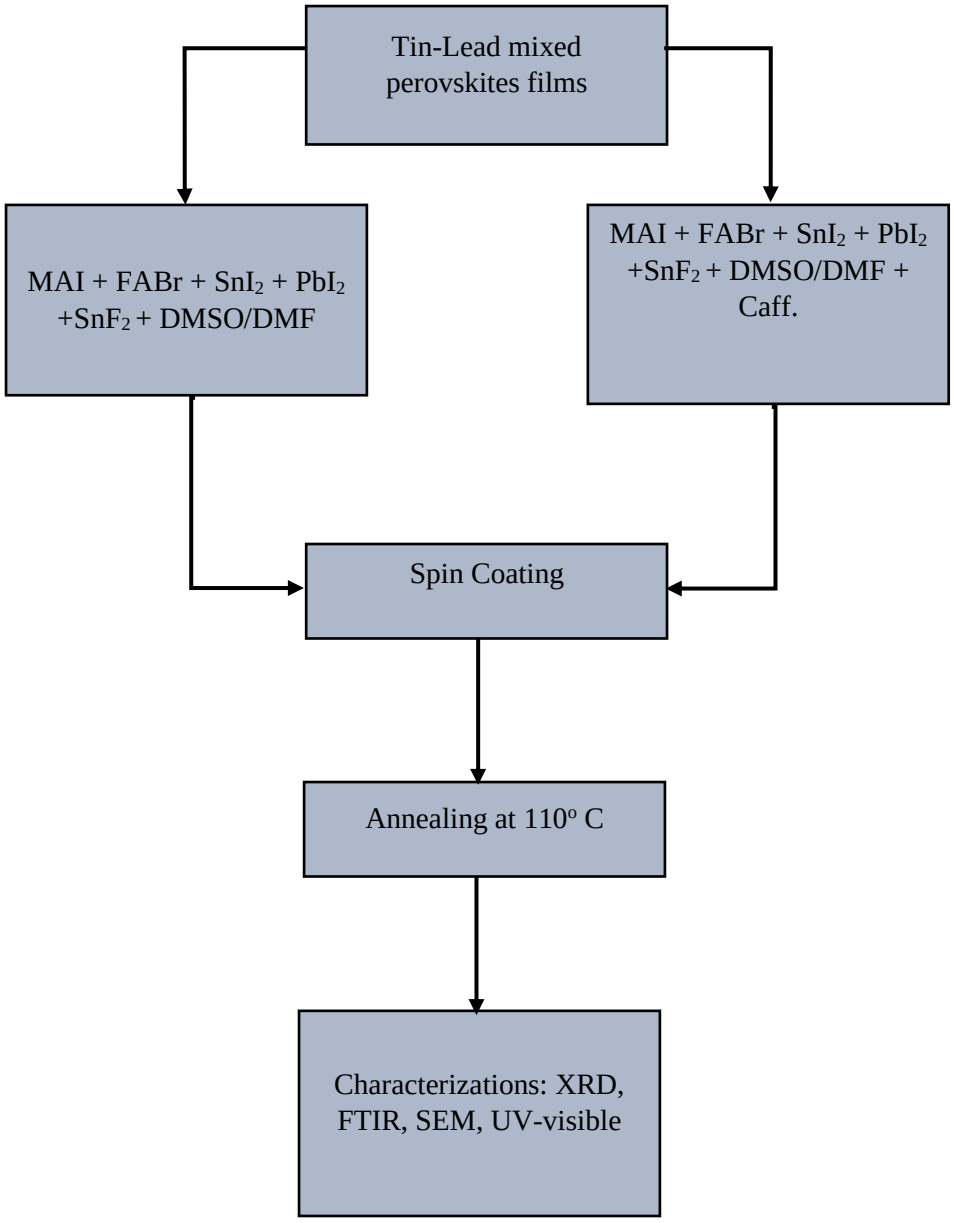
Tin-Lead mixed perovskites films
MAI + FABr + SnI_2 + PbI_2 +SnF_2 + DMSO/DMF
MAI + FABr + SnI_2 + PbI_2 +SnF_2 + DMSO/DMF + Caff.
Spin Coating
Annealing at 110^o C
Characterizations: XRD, FTIR, SEM, UV-visible

Summary

In this chapter, environment friendly alternatives such as tin and germanium elements for perovskite solar cell's applications are discussed. Undoubtedly, tin based perovskite materials offer unique optoelectronic properties and are considered front runners to replace toxic lead in PSCs. However, facile tin oxidation in ambient conditions and fast crystallization are the major challengers hampering their photovoltaic performance. Both of these problems have roots to the elemental tin which is unstable in the ambient environment hand has higher acidity as compared to lead. To overcome the tin oxidation problem, tin halides are frequently used as Sn^{2+} compensators. But still, the performance is not satisfactory. For the last few years, mixed tin-lead based perovskite materials have shown great potential for solar cell applications to mitigate lead toxicity along with narrow bandgap suitable for tandem applications.

References

[1] A. Kojima, K. Teshima, Y. Shirai, and T. Miyasaka, "Organometal halide perovskites as visible-light sensitizers for photovoltaic cells," *J. Am. Chem. Soc.*, vol. 131, no. 17, pp. 6050–6051, 2009, doi: 10.1021/ja809598r.

[2] H. Min *et al.*, "Perovskite solar cells with atomically coherent interlayers on SnO2 electrodes," *Nature*, vol. 598, no. 7881, pp. 444–450, 2021, doi: 10.1038/s41586-021-03964-8.

[3] J. Briffa, E. Sinagra, and R. Blundell, "Heavy metal pollution in the environment and their toxicological effects on humans," *Heliyon*, vol. 6, no. 9, p. e04691, 2020, doi: 10.1016/j.heliyon.2020.e04691.

[4] G. Schileo and G. Grancini, "Lead or no lead? Availability, toxicity, sustainability and environmental impact of lead-free perovskite solar cells," *J. Mater. Chem. C*, vol. 9, no. 1, pp. 67–76, 2021, doi: 10.1039/d0tc04552g.

[5] Y. G. Yoo *et al.*, "Evaluating the environmental impact of the lead species in perovskite solar cells via environmental-fate modeling," *J. Ind. Eng. Chem.*, vol. 70, pp. 453–461, 2019, doi: 10.1016/j.jiec.2018.11.008.

[6] I. R. Benmessaoud *et al.*, "Health hazards of methylammonium lead iodide based perovskites: Cytotoxicity studies," *Toxicol. Res. (Camb).*, vol. 5, no. 2, pp. 407–419, 2016, doi: 10.1039/c5tx00303b.

[7] A. Babayigit, A. Ethirajan, M. Muller, and B. Conings, "Toxicity of organometal halide perovskite solar cells," *Nat. Publ. Gr.*, vol. 15, no. 3, pp. 247–251, 2016, doi: 10.1038/nmat4572.

[8] X. Li, F. Zhang, J. Wang, J. Tong, T. Xu, and K. Zhu, "On-device lead-absorbing tapes for sustainable perovskite solar cells," *Nat. Sustain.*, 2021, doi: 10.1038/s41893-021-00789-1.

[9] X. Xiao *et al.*, "Lead-adsorbing ionogel-based encapsulation for impact-resistant , stable , and lead-safe perovskite modules," no. October, pp. 1–10, 2021.

[10] S. Chen, Y. Deng, X. Xiao, S. Xu, P. N. Rudd, and J. Huang, "Preventing lead leakage with built-in resin layers for sustainable perovskite solar cells," *Nat. Sustain.*, vol. 4, no. 7, pp. 636–643, 2021, doi: 10.1038/s41893-021-00701-x.

[11] B. Niu *et al.*, "Mitigating the Lead Leakage of High-Performance Perovskite Solar Cells via in Situ Polymerized Networks," *ACS Energy Lett.*, vol. 6, no. 10, pp. 3443–3449, 2021, doi: 10.1021/acsenergylett.1c01487.

[12] Y. Jiang *et al.*, "halide perovskite solar modules using self-healing polymer-based encapsulation," *Nat. Energy*, vol. 4, no. July, 2019, doi: 10.1038/s41560-019-0406-2.

[13] N. K. Noel *et al.*, "Environmental Science for photovoltaic applications †," *Energy Environ. Sci.*, vol. 7, pp. 3061–3068, 2014, doi: 10.1039/C4EE01076K.

[14] W. Ming, H. Shi, and M. H. Du, "Large dielectric constant, high acceptor density, and deep electron traps in perovskite solar cell material CsGeI3," *J. Mater. Chem. A*, vol. 4, no. 36, pp. 13852–13858, 2016, doi: 10.1039/c6ta04685a.

[15] A. M. Ganose, C. N. Savory, and D. O. Scanlon, "Beyond methylammonium lead iodide: prospects for the emergent field of ns2 containing solar absorbers," *Chem. Commun.*, vol. 53, no. 1, pp. 20–44, 2017, doi: 10.1039/c6cc06475b.

[16] Y. Bekenstein *et al.*, "The Making and Breaking of Lead-Free Double Perovskite Nanocrystals of Cesium Silver–Bismuth Halide Compositions," *Nano Lett.*, vol. 18, pp. 3502–3508, 2018, doi: 10.1021/acs.nanolett.8b00560.

[17] F. Yang *et al.*, "Magnesium-Doped MAPbI3 Perovskite Layers for Enhanced Photovoltaic Performance in Humid Air Atmosphere," *ACS Appl. Mater. Interfaces*, vol. 10, no. 29, pp. 24543–24548, 2018, doi: 10.1021/acsami.8b06619.

[18] M. Pham *et al.*, “Bismuth perovskite as a viable alternative to Pb perovskite solar cells : device simulations to delineate critical efficiency dynamics,” *J. Mater. Sci. Mater. Electron.*, no. 0123456789, 2019, doi: 10.1007/s10854-019-01275-3.
[19] Y. Zhang, L. Liao, and Y. Yang, “Composition Stoichiometry of Cs2AgBiBr6 Films for Highly Efficient Lead-Free Perovskite Solar Cells,” *Nano Lett.*, vol. 19, pp. 2066–2073, 2019, doi: 10.1021/acs.nanolett.9b00238.
[20] J. Huang, S. Zou, J. Lin, Z. Liu, and M. Qi, “Ultrathin lead-free double perovskite cesium silver bismuth bromide nanosheets,” *Nano Res.*, vol. 14, no. 11, pp. 4079–4086, 2021, doi: 10.1007/s12274-021-3343-x.
[21] N. Phung *et al.*, “The Doping Mechanism of Halide Perovskite Unveiled by Alkaline Earth Metals,” *J. Am. Chem. Soc.*, vol. 142, no. 5, pp. 2364–2374, 2020, doi: 10.1021/jacs.9b11637.
[22] M. Palummo, D. Varsano, E. Berríos, K. Yamashita, and G. Giorgi, “Halide pb-free double-perovskites: Ternary vs. quaternary stoichiometry,” *Energies*, vol. 13, no. 14, pp. 1–28, 2020, doi: 10.3390/en13143516.
[23] K. Eckhardt, V. Bon, J. Getzschmann, J. Grothe, F. M. Wisser, and S. Kaskel, “Crystallographic insights into (CH3NH3)3(Bi2I9): A new lead-free hybrid organic-inorganic material as a potential absorber for photovoltaics,” *Chem. Commun.*, vol. 52, no. 14, pp. 3058–3060, 2016, doi: 10.1039/c5cc10455f.
[24] S. Chatterjee and A. J. Pal, “Influence of metal substitution on hybrid halide perovskites: Towards lead-free perovskite solar cells,” *J. Mater. Chem. A*, vol. 6, no. 9, pp. 3793–3823, 2018, doi: 10.1039/c7ta09943f.
[25] M. R. Filip and F. Giustino, “Computational Screening of Homovalent Lead Substitution in Organic-Inorganic Halide Perovskites,” *J. Phys. Chem. C*, vol. 120, no. 1, pp. 166–173, 2016, doi: 10.1021/acs.jpcc.5b11845.
[26] G. Kieslich, S. Sun, and A. K. Cheetham, “An extended Tolerance Factor approach for organic-inorganic perovskites,” *Chem. Sci.*, vol. 6, no. 6, pp. 3430–3433, Jun. 2015, doi: 10.1039/c5sc00961h.
[27] J. Zhang *et al.*, “Pb-Site Doping of Lead Halide Perovskites for Efficient Solar Cells,” *Sol. RRL*, vol. 4, no. 2, 2020, doi: 10.1002/solr.201900227.
[28] R. E. Brandt *et al.*, “Investigation of Bismuth Triiodide (BiI3) for Photovoltaic Applications,” *J. Phys. Chem. Lett.*, vol. 6, no. 21, pp. 4297–4302, 2015, doi: 10.1021/acs.jpclett.5b02022.
[29] M. Lyu *et al.*, “Organic–inorganic bismuth (III)-based material: A lead-free, air-stable and solution-processable light-absorber beyond organolead perovskites,” *Nano Res.*, vol. 9, no. 3, pp. 692–702, 2016, doi: 10.1007/s12274-015-0948-y.
[30] A. K. Baranwal *et al.*, “Lead-free perovskite solar cells using Sb and Bi-based A3B2X9 and A3BX6 crystals with normal and inverse cell structures,” *Nano Converg.*, vol. 4, no. 1, 2017, doi: 10.1186/s40580-017-0120-3.
[31] M. Lyu, D. K. Lee, and N. G. Park, “Effect of alkaline earth metal chloride additives BCl2(B = Mg, Ca, Sr and Ba) on the photovoltaic performance of FAPbI3based perovskite solar cells,” *Nanoscale Horizons*, vol. 5, no. 9, pp. 1332–1343, 2020, doi: 10.1039/d0nh00263a.
[32] S. M. Jain, T. Edvinsson, and J. R. Durrant, “Green fabrication of stable lead-free bismuth based perovskite solar cells using a non-toxic solvent,” *Commun. Chem.*, vol. 2, no. 1, pp. 1–7, 2019, doi: 10.1038/s42004-019-0195-3.
[33] P. Umari, E. Mosconi, and F. De Angelis, “Relativistic GW calculations on CH3 NH3 PbI 3 and CH3 NH3 SnI3 Perovskites for Solar Cell Applications,” *Sci. Rep.*, vol. 4, pp. 1–7, 2014, doi: 10.1038/srep04467.
[34] Z. Chen *et al.*, “Photoluminescence study of polycrystalline CsSnI3 thin films:

Determination of exciton binding energy," *J. Lumin.*, vol. 132, no. 2, pp. 345–349, 2012, doi: 10.1016/j.jlumin.2011.09.006.
[35] I. Chung *et al.*, "CsSnI 3: Semiconductor or metal? High electrical conductivity and strong near-infrared photoluminescence from a single material. High hole mobility and phase-transitions," *J. Am. Chem. Soc.*, vol. 134, no. 20, pp. 8579–8587, 2012, doi: 10.1021/ja301539s.
[36] F. Hao, C. C. Stoumpos, D. H. Cao, R. P. H. Chang, and M. G. Kanatzidis, "Lead-free solid-state organic-inorganic halide perovskite solar cells," *Nat. Photonics*, vol. 8, no. 6, pp. 489–494, 2014, doi: 10.1038/nphoton.2014.82.
[37] T. M. Koh *et al.*, "Formamidinium tin-based perovskite with low Eg for photovoltaic applications," *J. Mater. Chem. A*, vol. 3, no. 29, pp. 14996–15000, 2015, doi: 10.1039/c5ta00190k.
[38] M. H. Kumar *et al.*, "Lead-free halide perovskite solar cells with high photocurrents realized through vacancy modulation," *Adv. Mater.*, vol. 26, no. 41, pp. 7122–7127, 2014, doi: 10.1002/adma.201401991.
[39] P. Xu, S. Chen, H.-J. Xiang, X.-G. Gong, and S.-H. Wei, "Influence of Defects and Synthesis Conditions on the Photovoltaic Performance of Perovskite Semiconductor CsSnI 3," *Chem. Mater.*, vol. 26, no. 20, pp. 6068–6072, Oct. 2014, [Online]. Available: https://pubs.acs.org/doi/10.1021/cm503122j.
[40] T. Nakamura *et al.*, "Sn(IV)-free tin perovskite films realized by in situ Sn(0) nanoparticle treatment of the precursor solution," *Nat. Commun.*, vol. 11, no. 1, pp. 1–8, 2020, doi: 10.1038/s41467-020-16726-3.
[41] E. Jokar *et al.*, "Slow Passivation and Inverted Hysteresis for Hybrid Tin Perovskite Solar Cells Attaining 13.5% via Sequential Deposition," *J. Phys. Chem. Lett.*, vol. 12, no. 41, pp. 10106–10111, 2021, doi: 10.1021/acs.jpclett.1c03107.
[42] Y. Takahashi *et al.*, "Charge-transport in tin-iodide perovskite CH3NH 3SnI3: Origin of high conductivity," *Dalt. Trans.*, vol. 40, no. 20, pp. 5563–5568, 2011, doi: 10.1039/c0dt01601b.
[43] I. Chung, B. Lee, J. He, R. P. H. Chang, and M. G. Kanatzidis, "All-solid-state dye-sensitized solar cells with high efficiency," *Nature*, vol. 485, no. 7399, pp. 486–489, 2012, doi: 10.1038/nature11067.
[44] T. Shi *et al.*, "Effects of organic cations on the defect physics of tin halide perovskites," *J. Mater. Chem. A*, vol. 5, no. 29, pp. 15124–15129, 2017, doi: 10.1039/c7ta02662e.
[45] G. Xie, L. Xu, L. Sun, Y. Xiong, P. Wu, and B. Hu, "Insight into the reaction mechanism of water, oxygen and nitrogen molecules on a tin iodine perovskite surface," *J. Mater. Chem. A*, vol. 7, no. 10, pp. 5779–5793, 2019, [Online]. Available: http://xlink.rsc.org/?DOI=C8TA11705E.
[46] D. Meggiolaro, D. Ricciarelli, A. A. Alasmari, F. A. S. Alasmary, and F. De Angelis, "Tin versus Lead Redox Chemistry Modulates Charge Trapping and Self-Doping in Tin/Lead Iodide Perovskites," *J. Phys. Chem. Lett.*, vol. 11, no. 9, pp. 3546–3556, May 2020, doi: 10.1021/acs.jpclett.0c00725.
[47] L. Lanzetta *et al.*, "Degradation mechanism of hybrid tin-based perovskite solar cells and the critical role of tin (IV) iodide," *Nat. Commun.*, vol. 12, no. 1, pp. 1–11, 2021, doi: 10.1038/s41467-021-22864-z.
[48] T. Leijtens, R. Prasanna, A. Gold-Parker, M. F. Toney, and M. D. McGehee, "Mechanism of Tin Oxidation and Stabilization by Lead Substitution in Tin Halide Perovskites," *ACS Energy Lett.*, vol. 2, no. 9, pp. 2159–2165, Sep. 2017, doi: 10.1021/acsenergylett.7b00636.
[49] T. Bin Song *et al.*, "Importance of reducing vapor atmosphere in the fabrication of Tin-based perovskite solar cells," *J. Am. Chem. Soc.*, vol. 139, no. 2, pp. 836–842, 2017, doi:

10.1021/jacs.6b10734.
[50] H. Perovskite, M. A. Kamarudin, D. Hirotani, Z. Wang, and K. Hamada, “Suppression of Charge Carrier Recombination in Lead-Free Tin,” *J. Phys. Chem. Lett.*, vol. 10, pp. 5277–5283, 2019.
[51] D. Ricciarelli, D. Meggiolaro, F. Ambrosio, and F. De Angelis, “Instability of tin iodide perovskites: Bulk p-doping versus surface tin oxidation,” *ACS Energy Lett.*, vol. 5, no. 9, pp. 2787–2795, 2020, doi: 10.1021/acsenergylett.0c01174.
[52] K. Liang, D. B. Mitzi, and M. T. Prikas, “Synthesis and Characterization of Organic-Inorganic Perovskite Thin Films Prepared Using a Versatile Two-Step Dipping Technique,” 1998.
[53] F. Hao *et al.*, “Solvent-Mediated Crystallization of CH3NH3SnI3 Films for Heterojunction Depleted Perovskite Solar Cells,” *J. Am. Chem. Soc.*, vol. 137, no. 35, pp. 11445–11452, 2015, doi: 10.1021/jacs.5b06658.
[54] W. Liao *et al.*, “Lead-Free Inverted Planar Formamidinium Tin Triiodide Perovskite Solar Cells Achieving Power Conversion Efficiencies up to 6.22%,” *Adv. Mater.*, vol. 28, no. 42, pp. 9333–9340, 2016, doi: 10.1002/adma.201602992.
[55] T. Yokoyama *et al.*, “Overcoming Short-Circuit in Lead-Free CH3NH3SnI3 Perovskite Solar Cells via Kinetically Controlled Gas-Solid Reaction Film Fabrication Process,” *J. Phys. Chem. Lett.*, vol. 7, no. 5, pp. 776–782, 2016, doi: 10.1021/acs.jpclett.6b00118.
[56] K. Yamada, S. Funabiki, H. Horimoto, T. Matsui, T. Okuda, and S. Ichiba, “ Structural Phase Transitions of the Polymorphs of CsSnI 3 by Means of Rietveld Analysis of the X-Ray Diffraction ,” *Chemistry Letters*, vol. 20, no. 5. pp. 801–804, 1991, doi: 10.1246/cl.1991.801.
[57] A. G. Kontos *et al.*, “Structural Stability, Vibrational Properties, and Photoluminescence in CsSnI3 Perovskite upon the Addition of SnF2,” *Inorg. Chem.*, vol. 56, no. 1, pp. 84–91, 2017, doi: 10.1021/acs.inorgchem.6b02318.
[58] Z. Chen, J. J. Wang, Y. Ren, C. Yu, and K. Shum, “Schottky solar cells based on CsSnI 3 thin-films,” *Appl. Phys. Lett.*, vol. 101, no. 9, 2012, doi: 10.1063/1.4748888.
[59] J. H. Heo, J. Kim, H. Kim, S. H. Moon, S. H. Im, and K. H. Hong, “Roles of SnX2 (X = F, Cl, Br) Additives in Tin-Based Halide Perovskites toward Highly Efficient and Stable Lead-Free Perovskite Solar Cells,” *J. Phys. Chem. Lett.*, vol. 9, no. 20, pp. 6024–6031, 2018, doi: 10.1021/acs.jpclett.8b02555.
[60] K. P. Marshall, R. I. Walton, and R. A. Hatton, “Tin perovskite/fullerene planar layer photovoltaics: Improving the efficiency and stability of lead-free devices,” *J. Mater. Chem. A*, vol. 3, no. 21, pp. 11631–11640, 2015, doi: 10.1039/c5ta02950c.
[61] S. Gupta, T. Bendikov, G. Hodes, and D. Cahen, “CsSnBr3, A Lead-Free Halide Perovskite for Long-Term Solar Cell Application: Insights on SnF2 Addition,” *ACS Energy Lett.*, vol. 1, no. 5, pp. 1028–1033, 2016, doi: 10.1021/acsenergylett.6b00402.
[62] D. Moghe *et al.*, “All vapor-deposited lead-free doped CsSnBr3 planar solar cells,” *Nano Energy*, vol. 28, pp. 469–474, 2016, doi: 10.1016/j.nanoen.2016.09.009.
[63] K. P. Marshall, M. Walker, R. I. Walton, and R. A. Hatton, “Enhanced stability and efficiency in hole-transport-layer-free CsSnI 3 perovskite photovoltaics,” *Nat. Energy*, vol. 1, no. 12, pp. 1–9, 2016, doi: 10.1038/nenergy.2016.178.
[64] Y. Yu *et al.*, “Thermally evaporated methylammonium tin triiodide thin films for lead-free perovskite solar cell fabrication,” *RSC Adv.*, vol. 6, no. 93, pp. 90248–90254, 2016, doi: 10.1039/c6ra19476a.
[65] H. Do Kim, Y. Miyamoto, H. Kubota, T. Yamanari, and H. Ohkita, “Open-circuit voltage loss in CH3NH3SnI3 perovskite solar cells,” *Chem. Lett.*, vol. 46, no. 2, pp. 253–256, 2017, doi: 10.1246/cl.160994.
[66] T. Handa, T. Yamada, H. Kubota, S. Ise, Y. Miyamoto, and Y. Kanemitsu, “Photocarrier

Recombination and Injection Dynamics in Long-Term Stable Lead-Free CH3NH3SnI3 Perovskite Thin Films and Solar Cells," *J. Phys. Chem. C*, vol. 121, no. 30, pp. 16158–16165, 2017, doi: 10.1021/acs.jpcc.7b06199.

[67] A. Amat *et al.*, "Cation-induced band-gap tuning in organohalide perovskites: Interplay of spin-orbit coupling and octahedra tilting," *Nano Lett.*, vol. 14, no. 6, pp. 3608–3616, 2014, doi: 10.1021/nl5012992.

[68] T. M. Koh *et al.*, "Formamidinium-containing metal-halide: An alternative material for near-IR absorption perovskite solar cells," *J. Phys. Chem. C*, vol. 118, no. 30, pp. 16458–16462, 2014, doi: 10.1021/jp411112k.

[69] D. Sabba *et al.*, "Impact of anionic Br - substitution on open circuit voltage in lead free perovskite (CsSnI 3-x Br x) solar cells," *J. Phys. Chem. C*, vol. 119, no. 4, pp. 1763–1767, 2015, doi: 10.1021/jp5126624.

[70] Z. Zhao *et al.*, "Mixed-Organic-Cation Tin Iodide for Lead-Free Perovskite Solar Cells with an Efficiency of 8.12%," *Adv. Sci.*, vol. 4, no. 11, 2017, doi: 10.1002/advs.201700204.

[71] X. Liu, K. Yan, D. Tan, X. Liang, H. Zhang, and W. Huang, "Solvent engineering improves efficiency of lead-free tin-based hybrid perovskite solar cells beyond 9%," *ACS Energy Lett.*, vol. 3, no. 11, pp. 2701–2707, 2018, doi: 10.1021/acsenergylett.8b01588.

[72] X. L. Li, L. L. Gao, Q. Q. Chu, Y. Li, B. Ding, and G. J. Yang, "Green Solution-Processed Tin-Based Perovskite Films for Lead-Free Planar Photovoltaic Devices," *ACS Appl. Mater. Interfaces*, vol. 11, no. 3, pp. 3053–3060, 2019, doi: 10.1021/acsami.8b19143.

[73] T. Fujihara, S. Terakawa, T. Matsushima, C. Qin, M. Yahiro, and C. Adachi, "Fabrication of high coverage MASnI3 perovskite films for stable, planar heterojunction solar cells," *J. Mater. Chem. C*, vol. 5, no. 5, pp. 1121–1127, 2017, doi: 10.1039/c6tc05069g.

[74] E. H. Jung *et al.*, "Efficient, stable and scalable perovskite solar cells using poly(3-hexylthiophene)," *Nature*, vol. 567, no. 7749, pp. 511–515, 2019, doi: 10.1038/s41586-019-1036-3.

[75] L. Vinet and A. Zhedanov, "A 'missing' family of classical orthogonal polynomials," *J. Phys. A Math. Theor.*, vol. 44, no. 8, pp. 9019–9038, 2011, doi: 10.1088/1751-8113/44/8/085201.

[76] Y. Ogomi *et al.*, "CH3NH3SnxPb(1-x)I3 perovskite solar cells covering up to 1060 nm," *J. Phys. Chem. Lett.*, vol. 5, no. 6, pp. 1004–1011, 2014, doi: 10.1021/jz5002117.

[77] T. Krishnamoorthy *et al.*, "Lead-free germanium iodide perovskite materials for photovoltaic applications," *J. Mater. Chem. A*, vol. 3, no. 47, pp. 23829–23832, 2015, doi: 10.1039/c5ta05741h.

[78] I. Kopacic *et al.*, "Enhanced Performance of Germanium Halide Perovskite Solar Cells through Compositional Engineering," pp. 343–347, 2018, doi: 10.1021/acsaem.8b00007.

[79] B. Park, B. Philippe, X. Zhang, H. Rensmo, G. Boschloo, and E. M. J. Johansson, "Bismuth Based Hybrid Perovskites A 3 Bi 2 I 9 (A : Methylammonium or Cesium) for Solar Cell Application," vol. 9, pp. 6806–6813, 2015, doi: 10.1002/adma.201501978.

[80] A. Manuscript, "Materials Chemistry A," 2017, doi: 10.1039/C7TA06679A.

[81] F. Hao, C. C. Stoumpos, R. P. H. Chang, and M. G. Kanatzidis, "Anomalous Band Gap Behavior in Mixed Sn and Pb Perovskites Enables Broadening of Absorption Spectrum in Solar Cells," 2014, doi: 10.1021/ja5033259.

[82] L. Li *et al.*, "High efficiency planar Sn-Pb binary perovskite solar cells: controlled

growth of large grains via a one-step solution fabrication process," *J. Mater. Chem. C*, vol. 5, no. 9, pp. 2360–2367, 2017, doi: 10.1039/c6tc05325d.

[83] G. Kapil *et al.*, "Highly Efficient 17.6% Tin–Lead Mixed Perovskite Solar Cells Realized through Spike Structure," *Nano Lett.*, vol. 18, pp. 3600–3607, 2018, doi: 10.1021/acs.nanolett.8b00701.

Chapter 3 Introduction to Deposition and Characterization Techniques

This chapter underlines an introduction of the thin film deposition and characterization techniques used to study optoelectronic properties of the perovskite films. Further, it also describes the working principal of these techniques.

3.1 Spin coating

Spin coating (SC) is a low cost wet thin film coating technique which utilizes liquid based solution precursors and disperse them uniformly on the substrates to obtain wet thin films. Usually, SC is used to achieve very thin film thickness usually in the regime of nanoscale.[1] Moreover, the easy processing and competitive cost make this technique more feasible research and laboratory scale level.

3.1.1 Working principal

SC working mechanism is classified into four steps, i.e., i) Deposition ii) Spin up , iii) Spin off and iv) Evaporation. In step-I, the precursors are dropped onto the flat substrate at low spin speed to disperse solution precursors under the influence of the centrifugal force. In step-II, the spin speed is raised to the desired spinning speed. At this stage, the precursor or fluid on the substrate may be spinning at a different speed than the substrate itself. Then, in step-III, the extra fluid swung off from the substrate and the wet film start changing its colour indicating that the drying process of the thin film has started. Finally, in step-IV, the fluid speed and the substrate speech are matched which results in the thinning of the film because of the evaporation of the solvent as shown in Figure3a.[2] Spinning speed and ramping rate of the SC process play significant role to modulate thickness of the film.

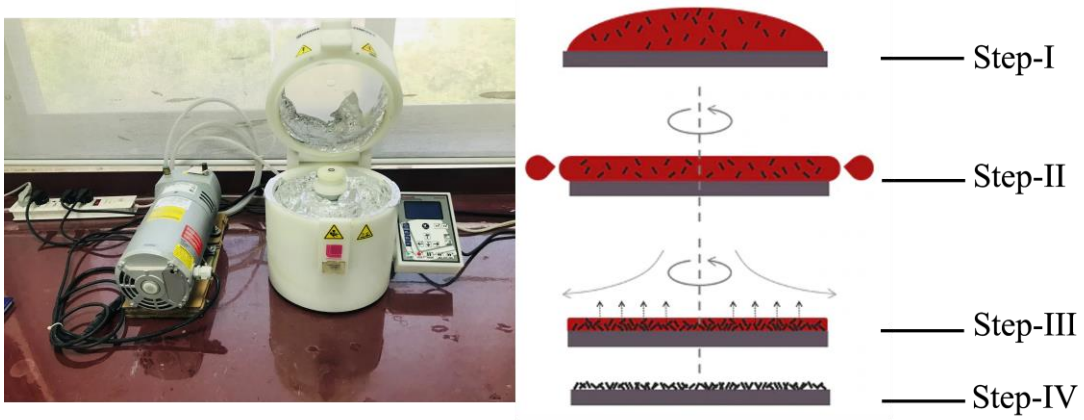

Figure 3.1 Image of spin coater instrument and schematic diagram of working mechanism.[2]

3.2 Glovebox

Gloveboxes or commonly known as laboratory gloveboxes are mainly used to store ambient environment sensitive materials or perform sensitive fabrication processes which are difficult to be carried out in normal conditions. Actually, these devices create a closed environment which primarily a sealed and stable environment to protect sensitive material that can react with the air.[3] Normally, an artificial inert environment is created in gloveboxes using nitrogen or argon as an inert gas.

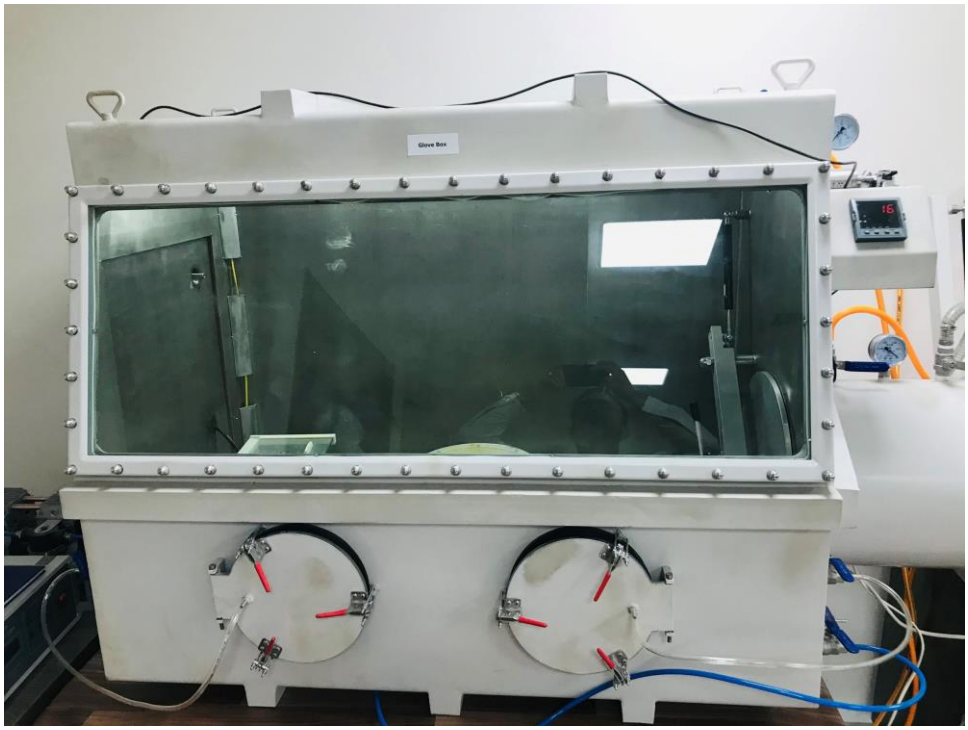

Figure 3.2 Image of humidity controlled glovebox.

A glovebox system consists of moisture (water) and oxygen sensors which show the levels of inside the glovebox. Moreover, it also comprises a heavy vacuum pump which is used to evacuate the glovebox chambers and to create an inert environment by purging nitrogen or argon gas.

3.3 Plasma cleaning

Plasma cleaning is a surface cleaning process which is used to remove very small organic/inorganic particles, oil etc. from the surface of the substrate just prior to the deposition of thin films. Normally substrates surfaces contain dust particles or organic residues which make these surfaces hydrophobic making it difficult to spin coat solution processable thin films. As a results, these surfaces are not covered completely during the deposition process. To counter this, a cleaning technique, known as plasma cleaning, is used to make the substrate surface more hydrophilic for the deposition of the thin films.

3.3.1 Working principal

Glass substrates, fluorine doped tin oxide (FTO) or indium doped tin oxide (ITO), are placed inside the plasma cleaner to remove small residual particles from the glass substrate surfaces. Then, the chamber is closed, and vacuum pump is turned on to completely evacuate the air present inside to create a vacuum. Afterwards, a mixture of oxygen and argon is injected inside the chamber to create a purple colour plasma for the removal of any contamination present on the surface of the ITO glass substrates. Normally, 10-20 minutes of the plasma treatment is suggested before the deposition of the thin films.

Figure 3.3 Image of plasma cleaner instrument.

3.4 UV-visible spectroscopy

UV-visible spectroscopy is an analytical tool which is used to study light spectrum response (absorbance, transmittance, and reflectance) of liquids and solid samples. It has been frequently used to probe materials such as semiconductors, thin film coatings, glass etc. UV-visible spectroscopy works on the principal of the Beer Lambart's law which states that the absorbance of a solution directly proportional to the concentration of the absorbing material present in the solution.[4]

Beer Lambart's law is stated by the following equation:

$$A = log\frac{I_O}{I} = \varepsilon lc = \alpha l$$

Where 'A' represents optical density or absorbance, I_o represents the incident light intensity, and 'I' represents transmitted light intensity, the molar extinction coefficient, 'ε', the concentration of a solution sample, 'c', and the absorption coefficient 'α'. Moreover, the fraction $\frac{I_O}{I}$ also represents transmittance.

3.4.1 Working principal

Generally, UV-visible spectrophotometers are of two types known as single beam and double beam based spectrophotometers. Single beam UV-visible spectrophotometers are divided into four major components as shown in Figure 3.

- Light source
- Monochromator
- Sample
- Detector

A continuous light beam is generated by light source enters into the monochromator chamber. Where the continuous light spectrum is split into discrete photons based on different wavelengths. Afterwards, the monochromatic light is directed on the sample where it is either absorbed, transmitted, or reflected back. Then, the response of the sample after interacting with the light beam is recorded by the designated detectors against the different wavelengths.[5]

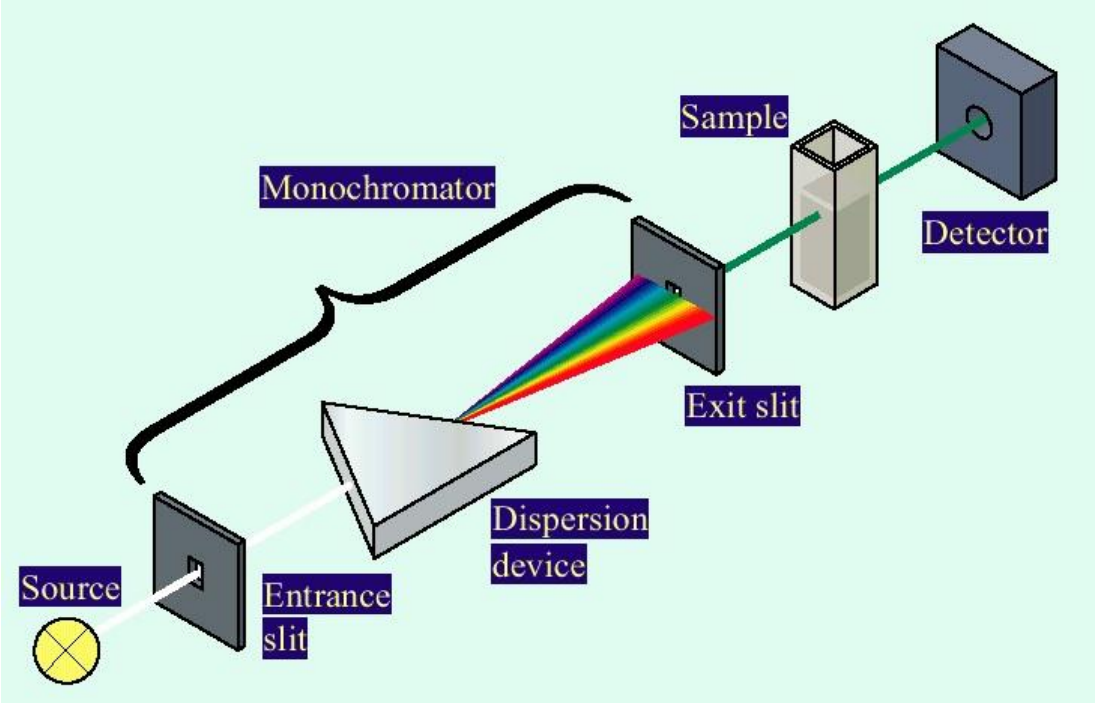

Figure 3.4 Schematic diagram of UV-visible spectrophotometer working mechanism.[5]

3.5 Fourier transform infrared spectroscopy

Fourier transform infrared spectroscopy (FTIR) is also an analytical technique to study the molecular interactions between various molecules in a sample either liquid or solids. FTIR has been frequently used in perovskite based photovoltaics to investigate the dopant interactions with the perovskite precursors. Moreover, it has been also widely applied in analytical chemistry to identify presence of various functional groups.

3.5.1 Working principal

The working principal of FTIR is more like similar to the UV-visible spectroscopy, except FTIR uses infrared light to probe the sample under the observation. Molecules are attached to each other by different types of chemical bonding, .i.e., ionic bond, covalent bond, Hydrogen bond and coordinate covalent bond etc. Whereases the frequency of vibrational motions of these bonds lies in the infrared regime. Generally, a Michaelson interferometer is used to measure the infrared response of the sample. An FTIR spectrometer is composed of a radiation source (infrared source), an interferometer and a detector. Infrared radiation source generates infrared radiations to pass from interferometer. Then, the interferometer splits the infrared radiation beams, creates an optical path difference between the two beams and generates the interference signal as a result of the optical path difference from the detector. The

detector records an IR response of the sample against the range of frequencies (wavenumber) ranges from 400- 4000 cm^{-1}.[6]

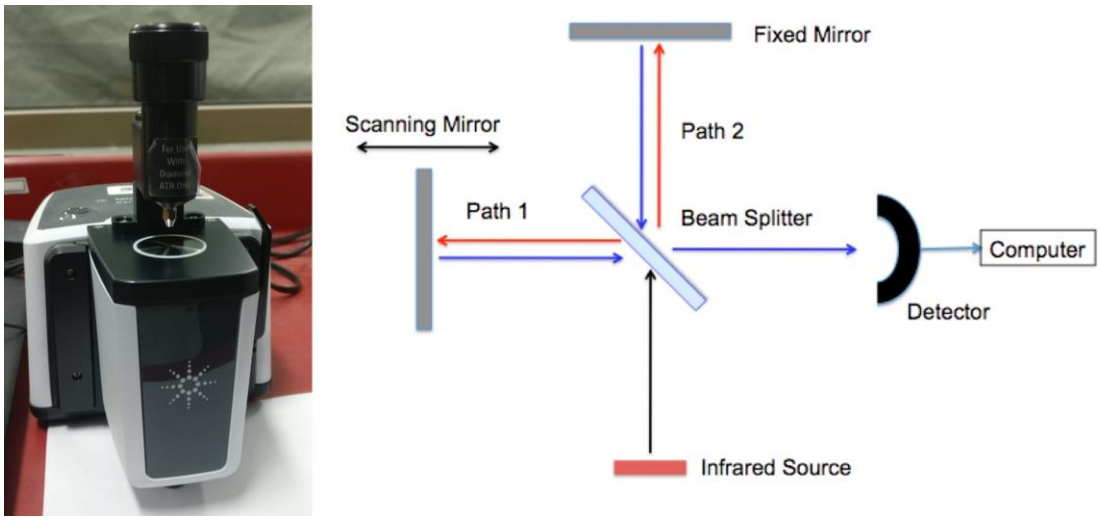

Figure 3.5 Image of Agilent FTIR interferometer and schematic illustration of its working mechanism.[7]

3.6 X-ray diffraction (XRD)

X-ray diffraction or XRD is a non-destructive analytical technique which is used to study the structural and crystallographic properties of the powdered and thin film based samples. It is also used to analyse crystal structure crystallinity of the samples. Moreover, it can also be used to identify the sample's crystalline phases, concentration profiles, film thickness and atomic patterns.

3.6.1 Working principal

In XRD, the collimated beam of X-rays that has wavelength in the range $\lambda \sim$ 0.5-2 Å is objected on a sample and then diffracted by the different crystalline phases as per relation the $\lambda = 2d\sin\theta$ (Bragg's law) where d is the interatomic spacing in the crystalline phase. XRD diffractometers are composed of three main units:

- X-ray tube
- Sample mounting stage
- X-ray detector

X-rays are generated inside the X-ray tubes where an electron beam is produced by heating a filament. Then these electrons are accelerated by applying voltage and bombarded on a target material. Afterwards, the electron beam that has sufficient energy dislodge the inner shell electrons of the target and as a result characteristic X-rays are produced. Then these X-rays are directed on the specimen at an angle of θ.

Whereas an X-ray detector is placed at angle of 2θ to record the diffracted X-rays. The geometry of the diffractometer is such that the sample mounting stage is continuously rotating in the path of the collimated X-ray beam. The instrument maintaining the angle and rotating the sample mounting stage is usually known as goniometer.[9]

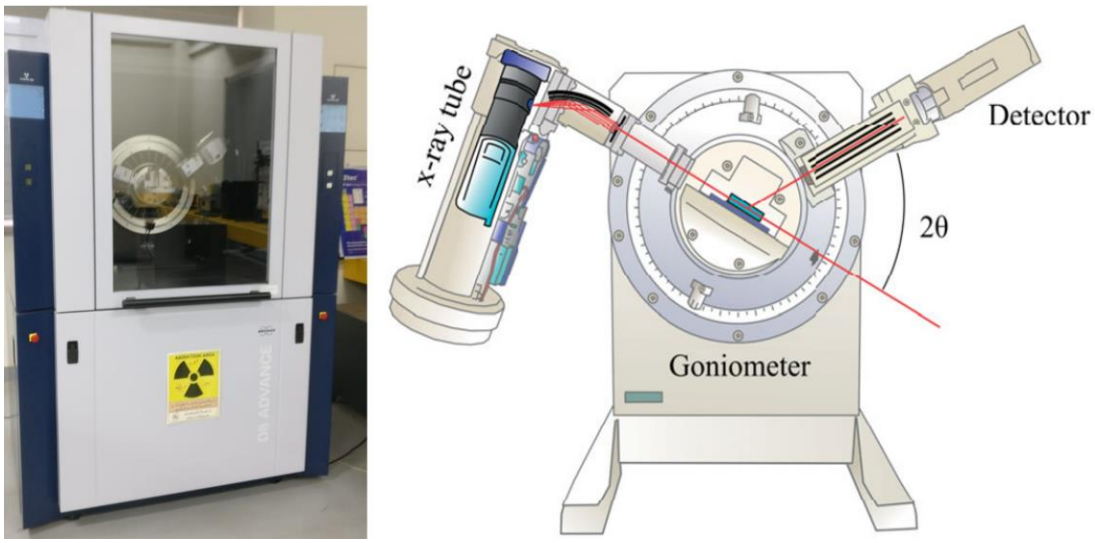

Figure 3.6 Image of XRD diffractometer and schematic diagram of its working mechanism.[10]

3.7 Scanning electron microscopy (SEM)

A scanning electron microscopy is a non-destructive imaging technique used to analyse or record an image of a specimen under observation. It provides information about the sample surface texture, morphology, and chemical composition. It has been frequently used to study solid powder or thin films based specimens.

3.7.1 Working principal

In the SEM, a focussed electron beam is bombarded on to the specimen and raster scanned over a small rectangular area. When the focussed beam of electrons interacts with specimen's surface, various types of phenomenon (emission of secondary electrons, photon emissions etc.) take place. These response can be efficiently recorded on a detector which ultimately forms an image based on the brightness of these electrons on traditionally used cathode ray tube. These images are just like the optical microscope images but with higher magnification with a depth of a nanoscale regime.[11] Generally, SEMs consist of the following components:

- Electron source gun
- Electron lenses
- Sample mounting stage

- Detectors, for all types of electrons or signals
- Display or output systems

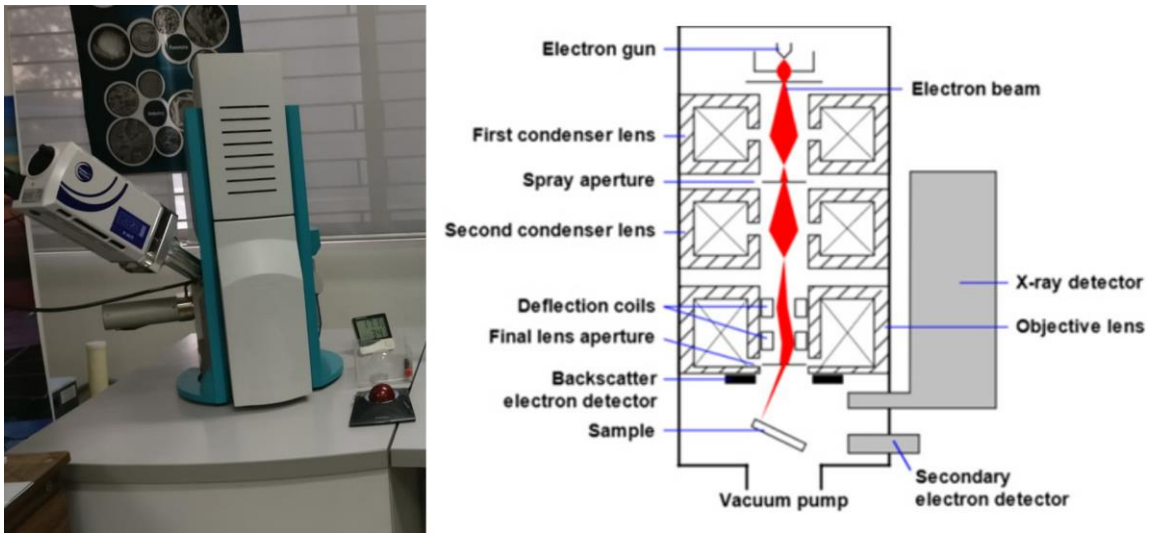

Figure 3.7 Image of SEM and schematic diagram of its working mechanism.[12]

Summary

This chapter can be divided into two sections: first section describes the processing techniques used and the second section illustrates the techniques used to characterize the mixed Sn-Pb based perovskite films. The processing techniques are explained, and the working principal of the equipment used i.e., spin coater and glovebox. In addition, state of the art characterization techniques such as XRD, FTIR, SEM etc. are discussed along with their structure and working principal.

References

[1] A. G. Emslie, F. T. Bonner, and L. G. Peck, “Flow of a viscous liquid on a rotating disk,” *J. Appl. Phys.*, vol. 29, no. 5, pp. 858–862, 1958, doi: 10.1063/1.1723300.

[2] “Spin Coating: Complete Guide to Theory and Techniques | Ossila.” https:// www.ossila.com/pages/spin-coating#spin-coating-thickness-equation

[3] “Glovebox Leaks, Box Design, Applications and More | Ossila.” https://www. ossila.com/pages/glove-box-application-notes

[4] “Beer-Lambert Law - an overview | ScienceDirect Topics.” https://www. sciencedirect.com/topics/engineering/beer-lambert-law

[5] “Instrument Design – UV-Vis Spectroscopy FAQ.”

[6] A. Dutta, Fourier Transform Infrared Spectroscopy, vol. 2. Elsevier Inc., 2017.

[7] “14. Fourier Transform Infrared Spectroscopy (FTIR) - Chemistry LibreTexts.”

[9] “X-ray Powder Diffraction (XRD).” https://serc.carleton.edu/msu_nanotech /methods/XRD.html

[10] B. Stefanov, Photocatalytic TiO2 thin films for air cleaning, no. January. 2015.

[11] “Scanning Electron Microscopy (SEM).” https://serc.carleton.edu/ research_ education/geochemsheets/techniques/SEM.html

[12] “Scanning Electron Microscopy - Nanoscience Instruments.” https:// www. nanoscience.com/techniques/scanning-electron-microscopy/

Chapter 4 Experimental Work

This chapter illustrates the experimental work performed to prepare the mixed Sn-Pb halide precursors, substrate preparation and the fabrication of the perovskite films. In addition, it also describes the parameters used to characterize these films.

4.1 Materials

All materials were used as received unless stated otherwise. Methylamine (CH_3NH_2) solution (33% wt. % in abs. ethanol) product no. 534102 from sigma Aldrich, Ethylene-diamine from Uni-CHEM, Hydrochloric acid (HCL) 35.5% aqueous solution and hydriodic acid (HI) solution (57% in water) were purchased from VWR international. Formamidinium bromide (FABr), tin iodide (SnI_2), tin fluoride (SnF_2), lead iodide (PbI_2), chlorobenzene (CB), titanium tetra-isopropoxide (TTIP), and mesoporous titanium dioxide paste were purchased from Sigma-Aldrich and anhydrous caff. (≥98.5%) was obtained from Carl Roth Int. Anhydrous dimethyl-formamide (DMF) and dimethyl-sulfoxide (DMSO) solvents were procured from Duksan Pure Chemicals Co. Ltd. Carbon powder was bought from DAEJUNG Chemicals.

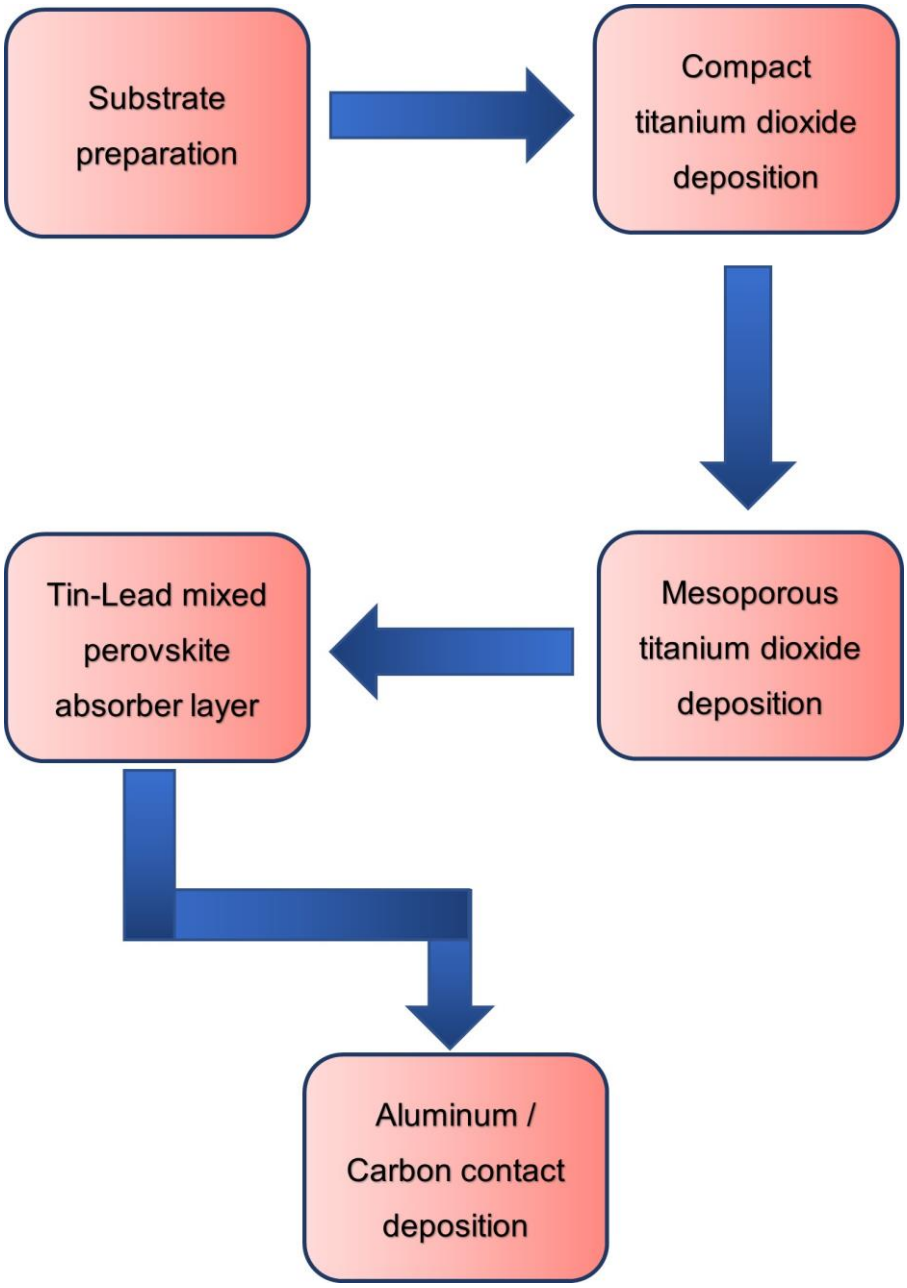

Figure 4.1 Block diagram of the methodology frame work.

4.2 Fabrication of Tin-lead mixed PSCs

4.2.1 Substrate preparation

Fluorine doped tin oxide (FTO) glass substrates were imported from Sigma-Aldrich. FTO glass substrates were patterned using zinc powder and 2M HCl solution. Afterwards, they were sequentially sonicated in deionized water, ethanol, and isopropyl alcohol for 10 minutes, respectively. After drying, they were further plasma cleaned for 10 minutes to remove any organic residue as shown in Figure 4.2.

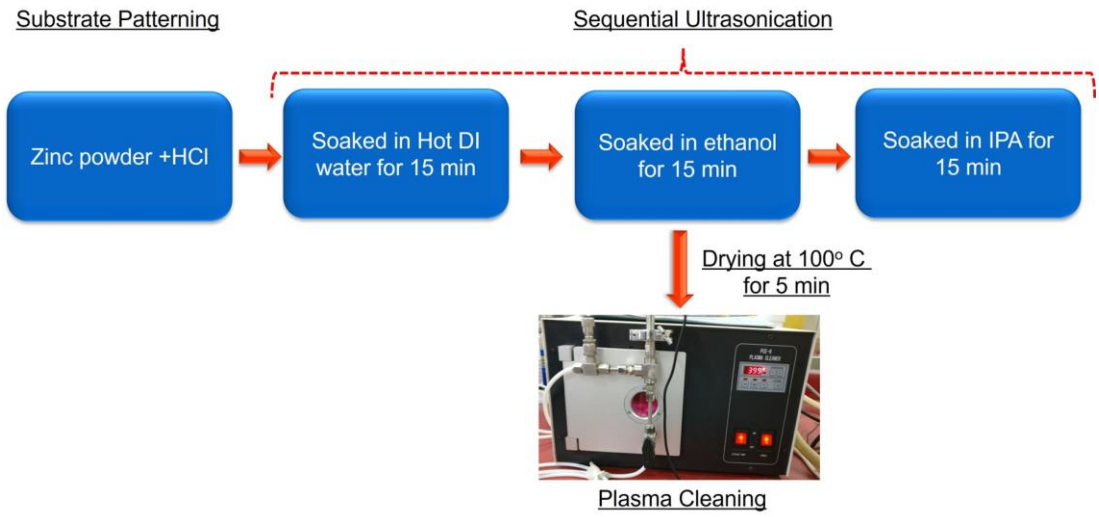

Figure 4.2 Schematic illustration of substrate cleaning and preparation.

4.3 Compact titanium dioxide layer preparation and deposition

Titanium dioxide (TiO_2) precursor solution was prepared by dissolving a mixture of 570 uL of TTIP in 2.53 ml of isopropanol (IPA) known as solution A and 2.28 uL of 2 M HCl in 2.53 ml of IPA known as solution B. Solution B was added dropwise slowly into solution A to maintain the acidic medium of the solution. Afterwards, the mixture of solution A and solution B was stirred for half hour to obtain a homogeneous solution. precursor solution was spin coated on FTO glass substrates for 30 s at 2000 rpms followed by annealing at 500 C for 30 minutes to obtain a compact TiO_2 thin film as shown in Figure 4.3.

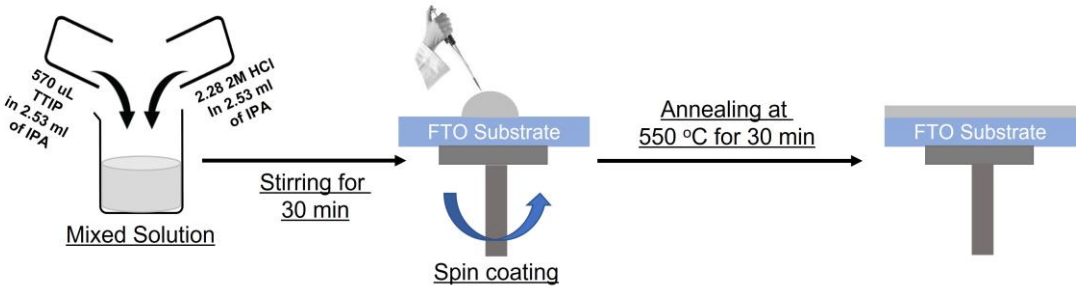

Figure 4.3 Schematic diagram of compact TiO_2 precursor deposition and film preparation.

4.4 Mesoporous TiO_2 layer preparation and deposition

For mesoporous TiO_2 deposition, mesoporous TiO_2 paste was diluted with ethanol in 1:8 ratio and spin-coated onto the c-TiO_2 layer for 20 s at 3000 rpm. After that, substrates were annealed at 520 C for 30 mins as shown in Figure 4.4.

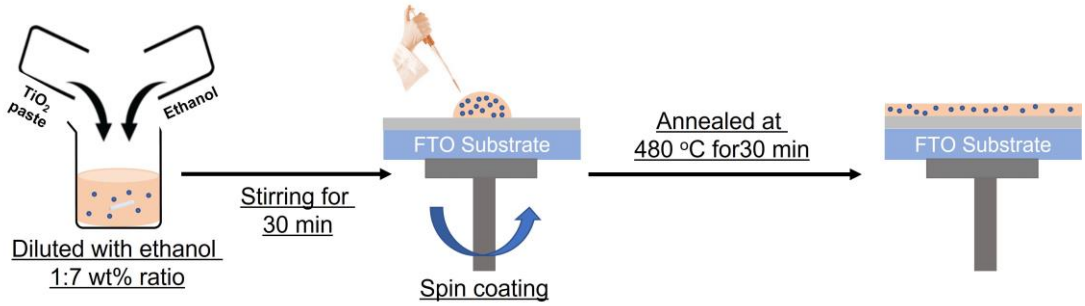

Figure 4.4 Schematic diagram of compact TiO_2 precursor deposition and film preparation

4.5 Synthesis of methylammonium iodide (MAI)

Methylammonium iodide was prepared following method reported elsewhere except the process was carried out in ambient conditions.10 ml of HI was added dropwise in the solution of 25 ml of methylamine and 100 ml ethanol and the temperature was kept at 0 °C for 3 hours under rigorous stirring to complete the chemical reaction. Afterwards, a yellow powder was separated through solvent evaporation in a rotary evaporator. Then, the product was washed out several times with copious amount of diethyl ether to remove impurities. As a result, a light-yellow powder was obtained and recrystallized with ethanol and was further dried in a vacuum oven at 60 °C as shown in Figure 4.5.

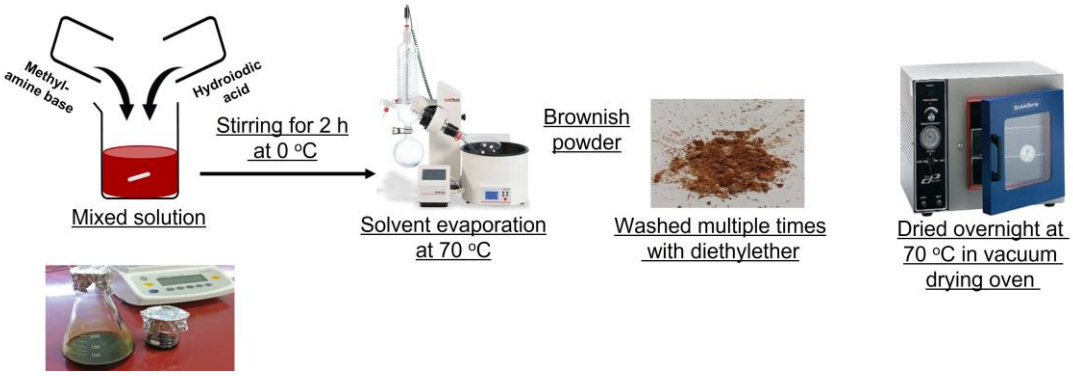

Figure 4.5 Synthesis of MAI precursors and powder.

4.6 Synthesis of ethylenediammonium diiodide

Ethylenediammonium-diiodide ($EDAI_2$) was obtained from reacting Ethylenediamine (en) with excess hydroiodic acid (to complete the chemical reaction) following the procedure reported elsewhere[6]. 25 ml of HI was slowly added to the 10 ml of Ethylenediammonium in an ice bath (Caution: the chemical reaction is highly exothermic) under continuous stirring for 3 hours. $EDAI_2$ precipitated out at the

bottom of the flask and a brownish powder was separated through rotary evaporator. Then, the produce was washed 5-times with diethyl ether and a white powder was recovered, which was further dried in a vacuum oven at 50o C for 24 hours.

4.7 Synthesis of ethylenediammonium dichloride

Ethylenediammonium-dichloride ($EDACl_2$) was prepared by the reaction of ethylenediamine with hydrochloric acid in a molar ratio 1:2 under ice bath at continuous stirring for 3 hours. As a result, $EDACl_2$ precipitated out at the bottom of the flask and a yellowish powder was separated through rotary evaporator, which was further washed three times with diethylether to remove impurities. Afterwards, the product was dried at 50o C for 24 hours in a vacuum oven.

4.8 Preparation of $FA_{0.2}MA_{0.8}Sn_{0.5}Pb_{0.5}I_{2.4}Br_{0.6}$ perovskite precursor solution

Mixed cation mixed halide Sn-Pb perovskite, $FA_{0.2}MA_{0.8}Sn_{0.5}Pb_{0.5}I_{2.4}Br_{0.6}$, precursor solution was prepared by dissolving FABr (0.2 mM), MAI (0.8 mM), PbI_2 (0.5 mM), SnI_2 (0.5 mM), SnF_2 (0.2 mM) in 1 ml of a mixed solvent system DMF: DMSO with a ratio 4:1, respectively, and stirred for overnight at 70 ^oC. Then, the solution was cooled down to room temperature before filtering with a 0.22 um polytetrafluoroethylene (PTFE) filter to remove undissolved particles. For caff. doped precursors, caff. concentration was gradually increased in molar ratio with SnI_2 from 0 mol% to 1.25 mol%, 2.5 mol% and 5 mol% as shown in Figure 4.6.

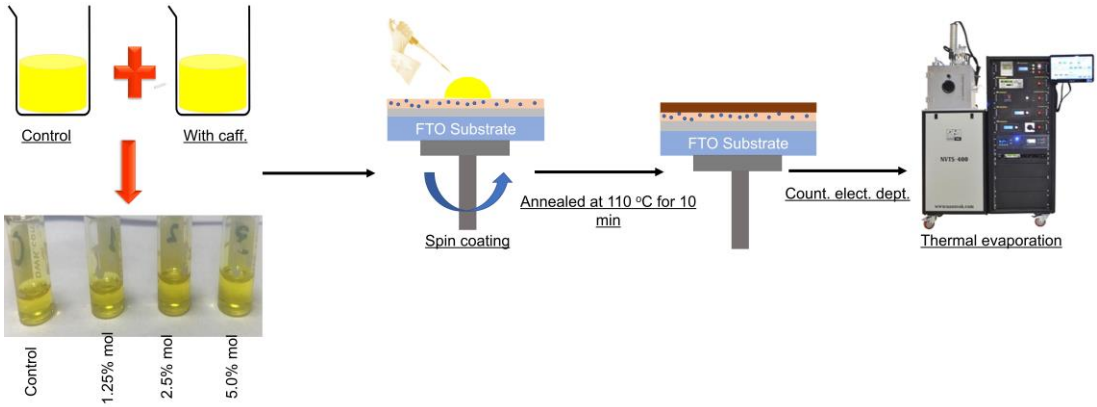

Figure 4.6 Schematic diagram of $FA_{0.2}MA_{0.8}Sn_{0.5}Pb_{0.5}I_{2.4}Br_{0.6}$ precursor synthesis and film deposition

4.9 Fabrication of $FA_{0.2}MA_{0.8}Sn_{0.5}Pb_{0.5}I_{2.4}Br_{0.6}$ perovskite absorber films

For the deposition of Sn-Pb mixed perovskite absorber layer, the TiO_2 coated FTO substrates were transferred into a glovebox where RH was kept under 10% for the perovskite film deposition. The complete process for the deposition of perovskite films is shown in the Figure 4.7 and video S1. 10 µL of perovskite solution was statically

spin-coated onto the glass substrates in two steps. The first step is 1000 rpm for 10 s and then the second step is 5000 rpm for 30 s. Meanwhile, 200 µL of CB antisolvent was dropped onto the substrates during the last 15 seconds before the end of the program. Afterward, the glass substrates were annealed at 110 ^{o}C for 20 mins to complete the perovskite phase conversion, as shown in Figure 4.7.

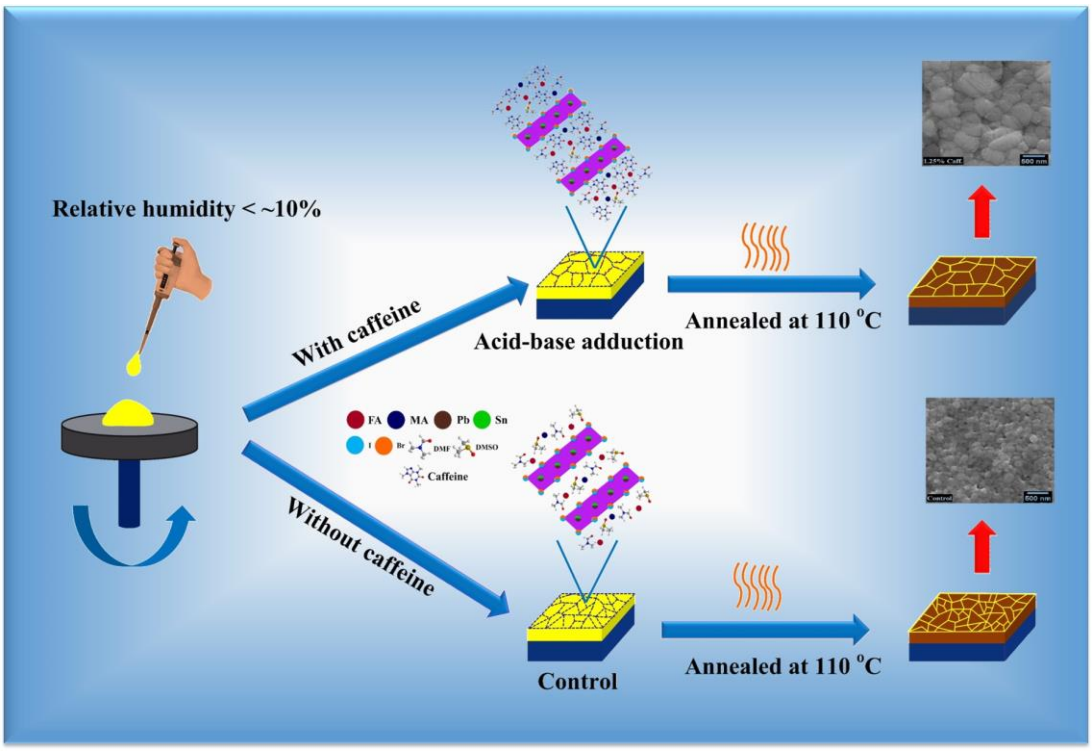

Figure 4.7 Schematic illustration of control and caff. doped Sn-Pb mixed perovskite fim deposition.

4.10 Film characterization

4.10.1 XRD

To study structural and crystallographic properties of Sn-Pb mixed perovskite films, the X-ray diffraction (XRD) technique was used. The XRD patterns were obtained using Bruker D8 Advanced with a 1.2/ min scan rate and 2θ range from 10o to 40o, using a CuKα radiation source (λ=1.54056 Å) with an excitation voltage of 40 kV and a current of 40 mA. X'Pert HighScore Plus software was used for analysing XRD data.

4.10.2 UV-visible absorption spectroscopy

For the measurement of optical properties, UV-visible absorbance spectra were recorded from the Shimadzu UV-3600i Plus spectrophotometer.

4.10.3 SEM

The surface morphology of the Sn-Pb mixed perovskite absorber films was taken using the Scanning Electron Microscopy (SEM) TESCAN-VEGA-3. EDX analysis was

carried out using the same equipment by adjusting the voltage at 20 kV and 15 mm width.

4.10.4 FTIR

To analyse inter-molecular interactions, Fourier-transform infrared spectroscopy (FTIR) studies were performed using CARY 630 FTIR, Agilent Technologies, USA. The diamond ATR module was used, and the wavenumber range was kept from 4000-640 cm-1.

Summary

This chapter covers the experimentation performed in this research work. First, the materials and their make. Then, concentrations of the materials used to prepare Sn-Pb mixed perovskites and afterwards the processing parameters along with complete description of the sample preparation. In addition, the parameters used to characterize the Sn-Pb mixed perovskite films are also provided.

Chapter 5 Results and Discussion

This chapter discusses the effect of caffeine doping on different optoelectronic properties meanwhile in their ambient fabrication. Further, it also includes a detail discussion of the results and provides justifications for them.

5.1 Fabrication of Sn-Pb mixed perovskite films

5.1.1 Dopant assisted change in morphology and interaction with Sn^{2+} and Pb^{2+} ions

Lead halide based PSCs are difficult to fabricate in an ambient environment owing to the uncontrolled crystallization of perovskite films due to the moisture present in the air. Water molecules tend to react with the perovskite precursors during the film formation and inhibit the proper growth of the grains in perovskite films.[1] Likewise, Sn-Pb mixed perovskite films also suffer through a similar fate even in the inert environment (H_2O< 0.1 ppm and O_2< 0.1 ppm). However, this behaviour is usually attributed to the higher acidity of Sn^{2+} resulting in the uncontrolled crystallization of Sn-Pb mixed perovskite films.[2] Lewis acid-base adduction has been reported as a successful technique to modulate the crystallization and growth of the perovskite film grains.[3] A caff. molecule contains two C=O functional groups, as shown in Figure 5.1 a. Moreover, it has also been frequently used as an antioxidant agent in food and biochemistry.[4],[5],[6],[7] The C=O functional groups of the caff., acting as Lewis base, can form an acid-base adduct with Pb^{2+} and Sn^{2+} ions in the precursors as seen in Figure 5.2 a.[8] This molecular interaction can turn into a molecular lock via chelation to enhance the activation energy of the nucleation, meanwhile, modulating the fast crystallization of the Sn-Pb mixed perovskite films.[9],[10].To verify this, we prepared $FA_{0.2}MA_{0.8}Sn_{0.5}Pb_{0.5}I_{2.4}Br_{0.6}$ perovskite films without (control) and with caff. additive (1.25 mol%, 2.5 mol%, and 5 mol%) and deposited them on glass substrates (Figure. 5.1 b).

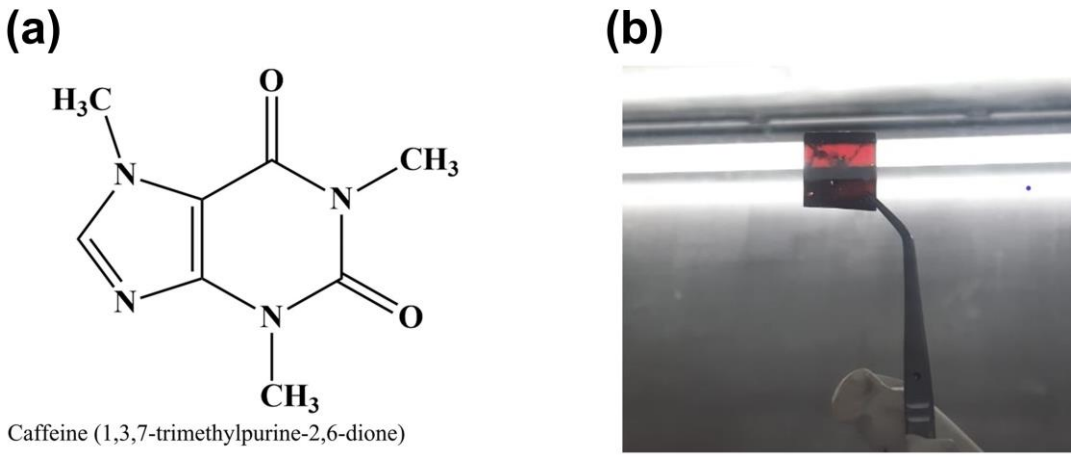

Figure 5.1 a) Structural formula of caffeine (1,3,7-trimethylpurine-2,6-dione) and b) Sn-Pb based perovskite film after annealing.

Figure 5.2 a represents the Fourier-transform infrared spectrum (FTIR) of the pure caff. powder, control $FA_{0.2}MA_{0.8}Sn_{0.5}Pb_{0.5}I_{2.4}Br_{0.6}$ and caff. doped $FA_{0.2}MA_{0.8}Sn_{0.5}Pb_{0.5}I_{2.4}Br_{0.6}$ perovskite films. For the pure caff. powder, stretching vibration peaks of the two C=O functional groups are observed at 1691 cm^{-1} and 1641 cm^{-1}, respectively.[11] However, control perovskite films do not show any peaks in this region. But, when caff. is incorporated into the perovskite films, as seen in Figure 5.2 b, only C=O group, present at the lower wavenumber 1641 cm^{-1}, take part in the molecular interaction with Pb^{2+} and Sn^{2+} ions resulting in a redshift from 1641 cm^{-1} to 1651 cm^{-1}. This is due to the conjugation of C=O group with C=C bond ensuing the delocalization of electrons. Whereas the peak at 1691 cm^{-1} remains at its original position as reported elsewhere.[9] This suggests that caff. stays in the films after the annealing, anticipating modulating the crystallization of $FA_{0.2}MA_{0.8}Sn_{0.5}Pb_{0.5}I_{2.4}Br_{0.6}$ perovskite absorber films.

.

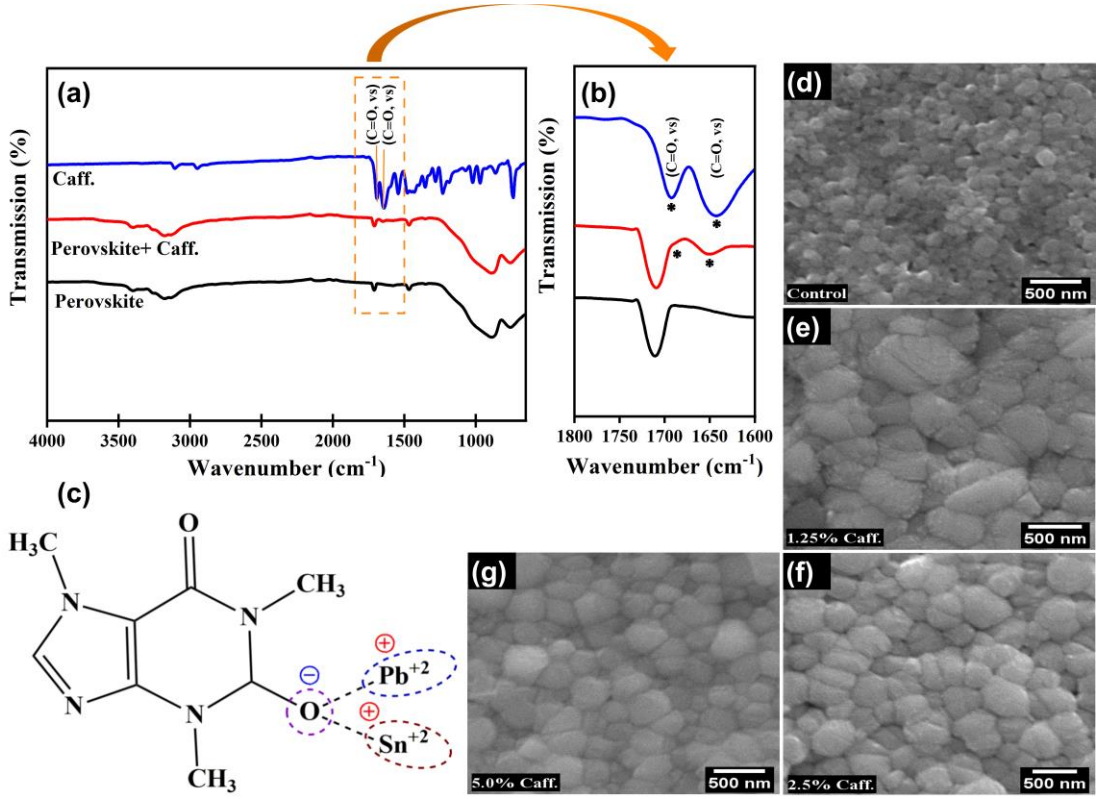

Figure 5.2 a) FTIR spectra of pure caff. powder, control, and caff. doped Sn-Pb perovskite films and b) Inset of the FTIR spectra indicating presence of caff. molecules in Sn-Pb perovskite films. c) Possible molecular interaction of C=O functional group with Pb^{2+} and Sn^{+2} ions in Sn-Pb perovskite precursors. SEM images of d) control, e) 1.25 mol%, f) 2.5 mol% and g) 5 mol% caff. doped Sn-Pb perovskite films, respectively.

To elucidate the role of caff. molecular locking with Pb^{2+} and Sn^{+2}, SEM images of the control and caff. doped $FA_{0.2}MA_{0.8}Sn_{0.5}Pb_{0.5}I_{2.4}Br_{0.6}$ perovskite films were recorded. As shown in Figure 5.2 d, control perovskite films contain many pinholes and very small grains attributed to the characteristic fast crystallization of Sn-Pb mixed perovskite films.[12], [13] Expectingly, as the concentration of caff. is increased to 1.25 mol%, the grain size is improved significantly which can be seen in Figure 5.2 e. However, with the further increase in the caff.'s concentration, the grain size starts decreasing due to the higher concentration of caff. confining the growth of large perovskite grains (Figure 5.2 f and g).[14],[15] To gain further insights into the caff. assisted increase of the grain size, energy-dispersive X-ray (EDX) image of the control and 1.25 mol% caff. doped perovskite films were performed. We observed that wt.% ratio of carbon has increased in caff. doped perovskite films as compared to the control films indicating incorporation of the caff. into perovskite films as shown in Figure. 5.3

a and 5.3 b. These results are in consistent with FTIR results (Figure 5.2 b and 5.2 c), implying that the C=O functional groups of caff. have successfully formed a molecular lock with Pb^{2+} and Sn^{2+} ions via an acid-base adduct formation to modulate the uncontrolled crystallization of $FA_{0.2}MA_{0.8}Sn_{0.5}Pb_{0.5}I_{2.4}Br_{0.6}$ perovskite absorber films by increasing the activation energy of the nucleation.

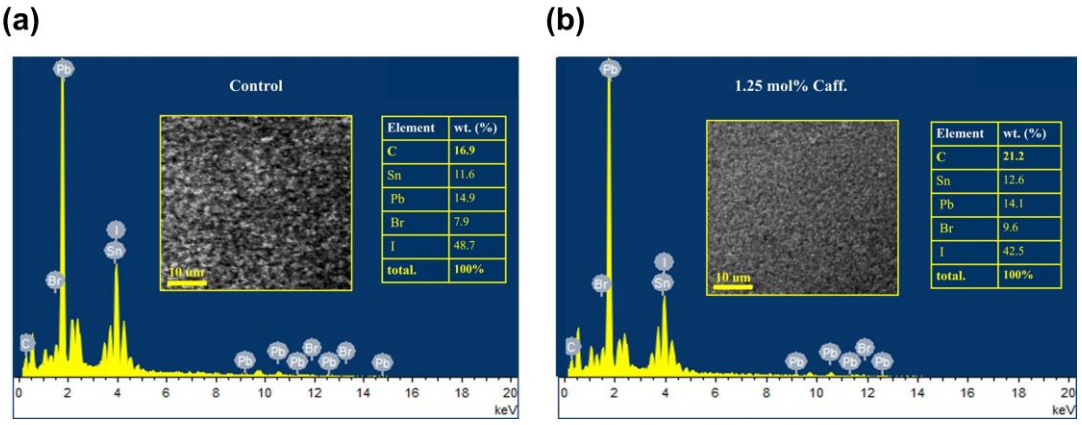

Figure 5.3 SEM images and EDX analysis of Sn-Pb perovskite absorber films of a) control and b) 1.25 mol% caff. doped.

5.1.2 Effect of caff. doping on structural properties o Sn-Pb mixed perovskite films

To investigate the crystallographic properties of $FA_{0.2}MA_{0.8}Sn_{0.5}Pb_{0.5}I_{2.4}Br_{0.6}$ perovskites, X-ray diffraction (XRD) of the thin films was performed. It is found that XRD patterns of control films show dominant perovskite peaks at 2θ values of 14.01° and 28.3° which can be associated to the (110) and (220) planes, respectively, as shown in Figure 5.4 a, no additional peak appears at 12.65° indicating complete conversion of perovskite phase.[16],[17] Moreover, we also observed that the intensity of XRD peaks gradually increased with the increase in the caff. doping concentration. To further probe the effect of caff. doping on perovskite film crystallinity, the fullwidth halfwave maximum (FWHM) of (110) plane peak at 14.01° is measured. It is found that the FWHM value of the (110) plane decreases systematically as the concentration of caff. is increased from 0% to 1.25%, afterward, FWHM values start increasing with further increase in the caff. doping concentrations as seen in Figure 5.4 b. This can also be observed in the increase of the crystallite size measured by the Scherer equation (Figure 5.5).[18]

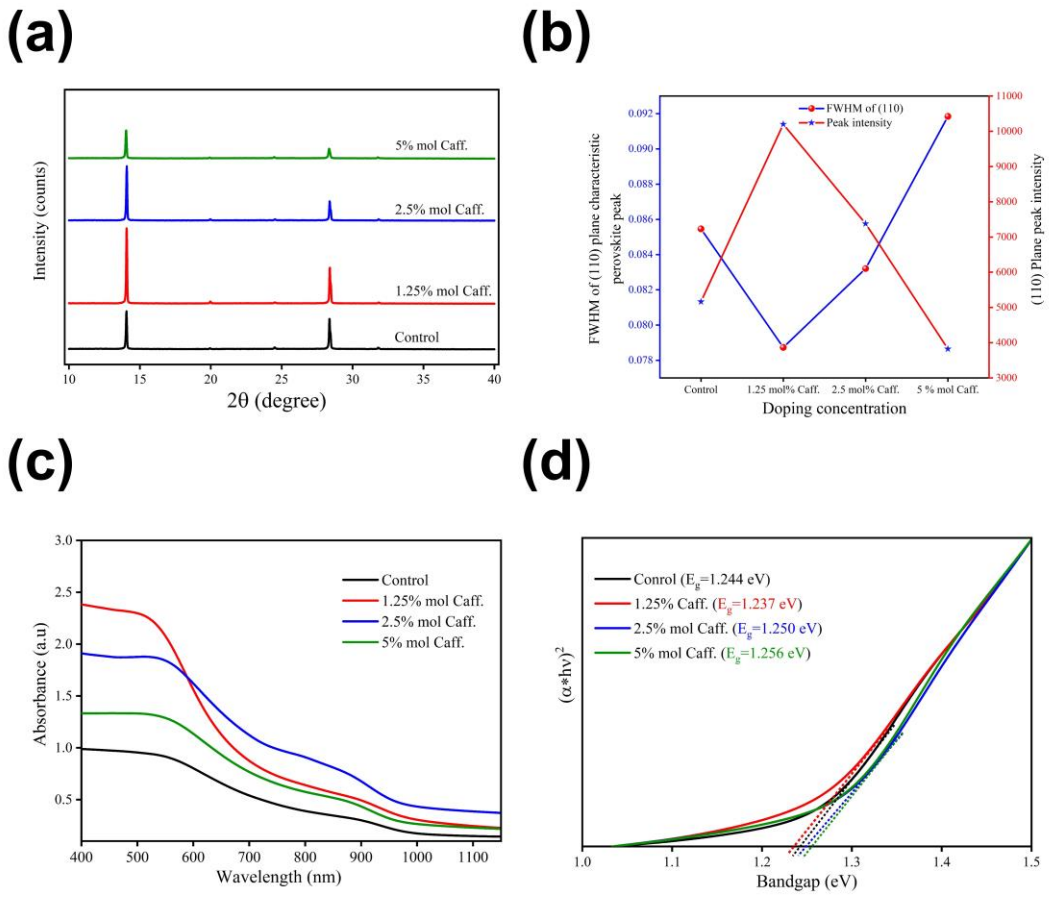

Figure 5.4 a) XRD patterns of control, 1.25 mol%, 2.5 mol% and 5 mol% caff. doped Sn-Pb perovskite films, b) FWHM and peak intensity of characteristic peak (110) at 14.09^{o} of control, 1.25 mol%, 2.5 mol%, and 5.0 mol% caff. doped Sn-Pb perovskite films. c) UV-visible absorbance spectrum and d) Tauc-plot of the control, 1.25 mol%, 2.5 mol% and 5 mol% mol caff. doped Sn-Pb perovskite films.

5.1.3 Effect of caff. doping on optical properties of Sn-Pb mixed perovskite films

To estimate the photoresponse of the ambient processed $FA_{0.2}MA_{0.8}Sn_{0.5}Pb_{0.5}I_{2.4}Br_{0.6}$ perovskite films, we performed UV-visible spectroscopy. The absorbance spectrum of the control and caff. doped Sn-Pb mixed perovskite films are shown in Figure 5.4 c). The absorption of $FA_{0.2}MA_{0.8}Sn_{0.5}Pb_{0.5}I_{2.4}Br_{0.6}$ perovskite films is gradually enhanced as the caff. concentration is increased from 0 mol% to 5 mol%. Under optimum caff. doping concentration, 1.25 mol% caff., the absorbance is maximum which is in good agreement with the improved grain size and enhanced crystallinity of the $FA_{0.2}MA_{0.8}Sn_{0.5}Pb_{0.5}I_{2.4}Br_{0.6}$ perovskite absorber films. Moreover, for 1.25 mol% caff. doped $FA_{0.2}MA_{0.8}Sn_{0.5}Pb_{0.5}I_{2.4}Br_{0.6}$ perovskite films, the absorption onset is redshifted relative to the control perovskite films which can be associated with the antioxidant properties of caff. stabilizing Sn^{2+}.[19] These observations are further corroborated by

tauc's plot, where the lowest bandgap is obtained for 1.25 mol% caff. doped $FA_{0.2}MA_{0.8}Sn_{0.5}Pb_{0.5}I_{2.4}Br_{0.6}$ perovskite films, as shown in Figure 5.4 d).

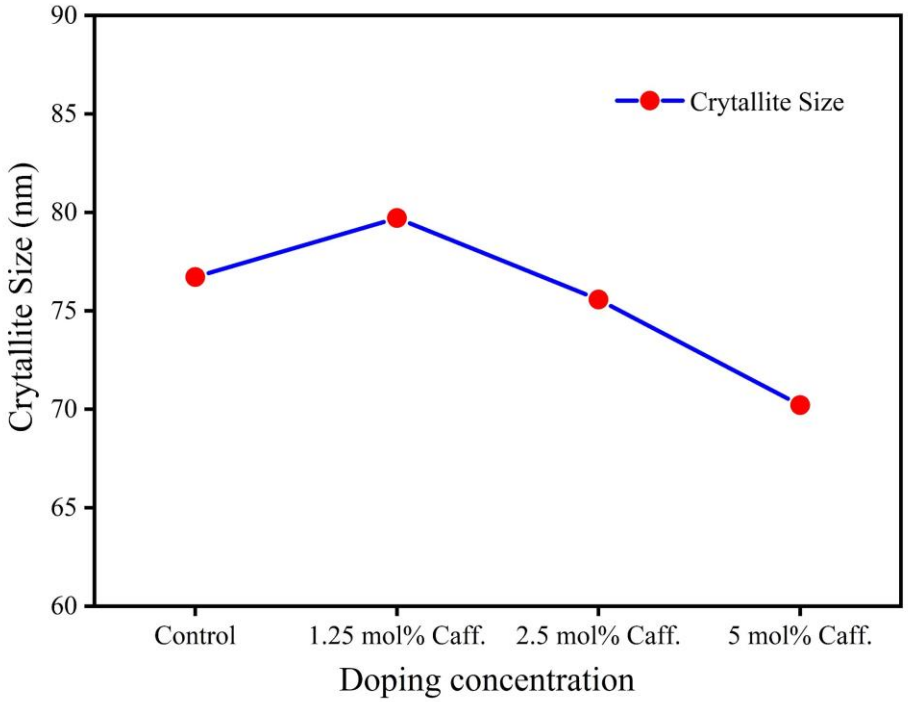

Figure 5.5 Change in crystallite size for the control, 1.25 mol%, 2.5 mol%, and 5.0 mol% caff. doped Sn-Pb perovskite films.

5.1.4 Effect of caff. doping on trap-states of Sn-Pb mixed perovskite films

To further quantify the effect of caff. doping on the electronic quality of the $FA_{0.2}MA_{0.8}Sn_{0.5}Pb_{0.5}I_{2.4}Br_{0.6}$ perovskite films, we determine Urbach energy (E_u) for the control and caff. doped Sn-Pb mixed perovskite films. E_u, also known as Urbach tail, states energetic disorder near the band edges (valence and conduction band) due to the presence of the localized states which is measured by linear fitting ln (α) versus photon energy (hγ) using a relation $\alpha = \alpha_0 * \exp\left(^{E}/_{E_u}\right)$ where α is the absorption coefficient, E is photon energy, and E_u is Urbach energy.[20] We found that control $FA_{0.2}MA_{0.8}Sn_{0.5}Pb_{0.5}I_{2.4}Br_{0.6}$ perovskite films have E_u= 277 meV value, whereas 1.25 mol%, 2.5 mol% and 5 mol% caff. doped perovskite films have E_u= 229 meV, E_u= 244 meV and E_u= 262 meV values, as shown in Figure 5.6 a- d, respectively. The stated reduction in the E_u values is due to the passivation of trap states near the band edges of the bandgap.[21],[22] Although, caff. doping has shown decreasing trend in E_u, but the values are very high which can be associated to the Sn^{2+} in ambient conditions.

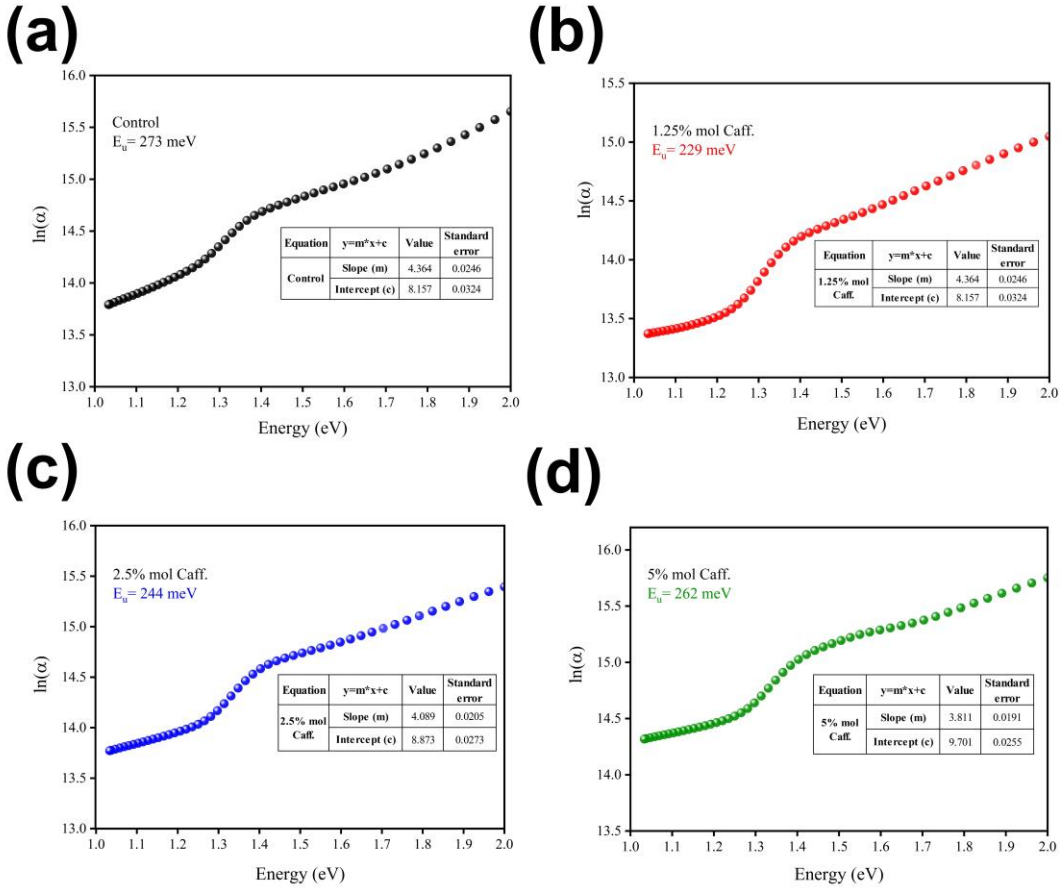

Figure 5.6 Urbach energy of (a) control, (b) 1.25 mol% (c) 2.5 mol% and (d) 5 mol% caff. doped Sn-Pb perovskite films (pictures of corresponding perovskite films are inset graph).

5.2 Additional research work done as research assistant under HEC NRPU project

5.2.1 XRD, UV-visible and SEM results of Methylammonium lead iodide based perovskite films

Methylammonium lead iodide ($MAPbI_3$) thin films were prepared by spin-coating precursors on glass substrates and annealed at 100 ^oC. XRD) was conducted to determine crystallographic properties of the $MAPbI_3$ perovskite films. XRD diffraction patterns revealed sharp peaks at 14.00^o and 28.36^o corresponding to the (110) and (220) planes indicating successful formation of the tetragonal perovskite structure as shown in Figure 5.7 a.[23], [24] To further corroborate formation of the perovskite structure, UV-visible spectroscopic studies were performed to analyse optical properties. As it can be seen in Figure 5.7 b, the absorption onset starts from 810 nm and ends at 760 nm attributed to the direct bandgap of the organic inorganic

lead iodide perovskites.[25] For optical bandgap estimation, Tauc plot was used as shown in Figure 5.7 c. The optical bandgap of MAPbI3 perovskite based films was around 1.53 eV.

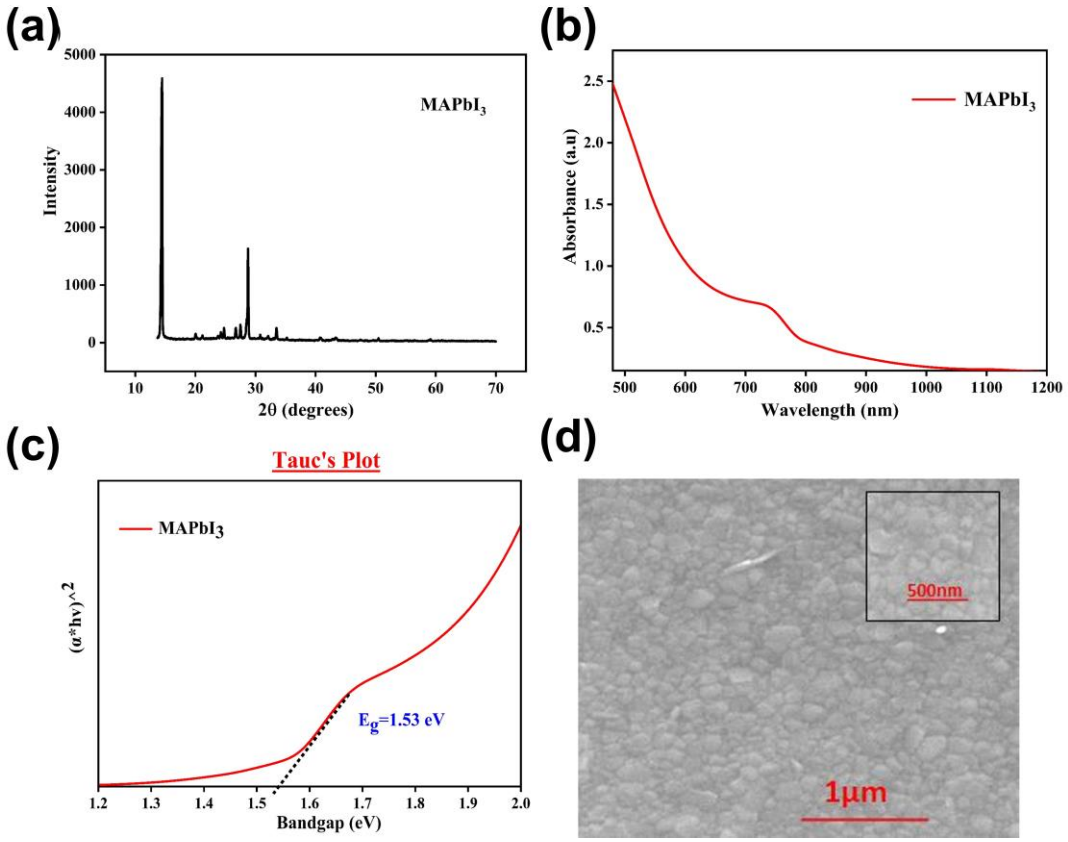

Figure 5.7 a) X-ray diffraction of $MAPbI_3$ based perovskite thin films, b) Absorption spectrum of $MAPbI_3$ perovskite thin films, c) tauc's plot of $MAPbI_3$ perovskite films and d) Scanning electron microscopy image of $MAPbI_3$ thin film.

Further, for scanning electron microscopy (SEM), $MAPbI_3$ precursor was drop casted on the FTO substrates and thin films were prepared. SEM images showed compact and uniform perovskite films as seen in Figure 5.7 d.

5.2.2 Fabrication and J-V Characterization of carbon based PSCs

Figure 5.8 a describes the complete fabrication process of HTL free carbon based PSCs. J-V measurements were conducted using standard 1.5 G A.M under 1 Sun illumination on solar cell simulator to record the PSC device response. For control PSC devices, where carbon powder simply sprinkled on the perovskite absorber layer, the power conversion efficiency was extremely low approximately 0.32% with other photovoltaic parameters, *i.e.*, fill factor, open-circuit voltage, short-current density values are 26%, 0.51 V and, 2.2 mAcm-2, respectively. On the other hand, for platinum coated counter FTO electrodes, the efficiency improved significantly up to

two folds as compared to control carbon powder based PSCs as shown in Figure 5.8 b. This difference in the performance be associated to the better contact between perovskite absorber layer platinum coated counter FTO resulting in lower interfacial resistances and significant increase in the performance. Figure 5.8 c shows the image of carbon based HTL free PSCs.

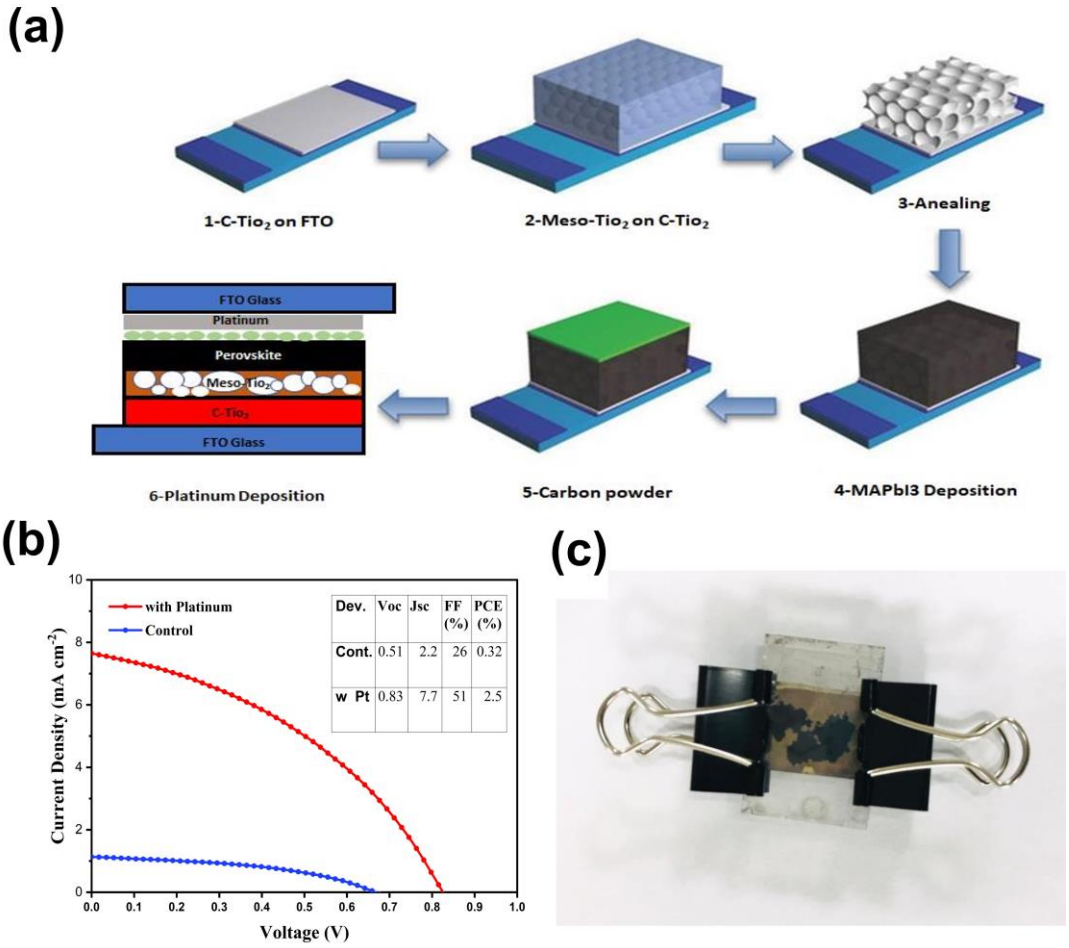

Figure 5.8 a) Schematic illustration of the complete PSC fabrication process, b) J-V curves of the controlled and platinum coated carbon-based PSCs, and c) image of the carbon-based PSCs.

Summary

This chapter presents results and discussion of an experimental study on additive assisted growth of $FA_{0.2}MA_{0.8}Sn_{0.5}Pb_{0.5}I_{2.4}Br_{0.6}$ narrow bandgap perovskite films employing a Lewis-base molecule, caffeine (1,3,7-trimethylpurine-,2,6-dione), having two carbonyl functional groups (C=O) in a low humidity environment (<~10%). The C=O interacts with metallic ions (Sn^{2+} and Pb^{2+}) via chelation to form an acid-base adduct, slowing down the fast crystallization of $FA_{0.2}MA_{0.8}Sn_{0.5}Pb_{0.5}I_{2.4}Br_{0.6}$ perovskite films. As a result, the grain size improves resulting in better structural and optical properties. In contrast, Urbach energy values showed higher electronic disorder near the band edges even upon caffein doping implying Sn^{4+} doping in ambient environment. This work accentuates the potential of the acid-base adduction to regulate uncontrolled crystallization of Sn-Pb perovskites in ambient environment.

References

[1] K. Zhang *et al.*, "A prenucleation strategy for ambient fabrication of perovskite solar cells with high device performance uniformity," *Nat. Commun.*, vol. 11, no. 1, pp. 1–11, 2020, doi: 10.1038/s41467-020-14715-0.

[2] R. M. I. Bandara, S. M. Silva, C. C. L. Underwood, K. D. G. I. Jayawardena, R. A. Sporea, and S. R. P. Silva, "Progress of Pb-Sn Mixed Perovskites for Photovoltaics: A Review," *Energy Environ. Mater.*, pp. 1–31, 2021, doi: 10.1002/eem2.12211.

[3] S. Wang *et al.*, "Lewis acid/base approach for efficacious defect passivation in perovskite solar cells," *J. Mater. Chem. A*, vol. 8, no. 25, pp. 12201–12225, 2020, doi: 10.1039/d0ta03957h.

[4] S. Nakamura, O. Nishimura, H. Masuda, and S. Mihara, "Identification of Volatile Flavor Components of the Oil from Roasted Sesame Seeds," *Agric. Biol. Chem.*, vol. 53, no. 7, pp. 1891–1899, 1989, doi: 10.1271/bbb1961.53.1891.

[5] X. Shi, N. S. Dalal, and A. C. Jain, "Antioxidant behaviour of caffeine: Efficient scavenging of hydroxyl radicals," *Food Chem. Toxicol.*, vol. 29, no. 1, pp. 1–6, 1991, doi: 10.1016/0278-6915(91)90056-D.

[6] A. Farah and C. M. Donangelo, "Phenolic compounds in coffee," *Brazilian J. Plant Physiol.*, vol. 18, no. 1, pp. 23–36, 2006, doi: 10.1590/S1677-04202006000100003.

[7] A. Yashin, Y. Yashin, J. Y. Wang, and B. Nemzer, "Antioxidant and antiradical activity of coffee," *Antioxidants*, vol. 2, no. 4, pp. 230–245, 2013, doi: 10.3390/antiox2040230.

[8] L. Zhang, X. Liu, J. Li, and S. McKechnie, "Interactions between molecules and perovskites in halide perovskite solar cells," *Sol. Energy Mater. Sol. Cells*, vol. 175, no. July 2017, pp. 1–19, 2018, doi: 10.1016/j.solmat.2017.09.038.

[9] R. Wang *et al.*, "Caffeine Improves the Performance and Thermal Stability of Perovskite Solar Cells," *Joule*, pp. 1–14, 2019, doi: 10.1016/j.joule.2019.04.005.

[10] S. Wafee, B. H. Liu, and C. C. Leu, "Lewis bases: promising additives for enhanced performance of perovskite solar cells," *Mater. Today Energy*, vol. 22, p. 100847, Dec. 2021, doi: 10.1016/J.MTENER.2021.100847.

[11] R. Barbara and V. Aroulmoji, "FT-IR Study of the Hydration of Caffeine, Sucrose, and Their Mixtures in Water," *Water Prop. Food, Pharm. Biol. Mater.*, no. July 2016, pp. 623–632, 2020, doi: 10.1201/9781420001181-51.

[12] H. L. Zhu and W. C. H. Choy, "Crystallization, Properties, and Challenges of Low-Bandgap Sn–Pb Binary Perovskites," *Sol. RRL*, vol. 2, no. 10, pp. 1–18, 2018, doi: 10.1002/solr.201800146.

[13] W. Liao *et al.*, "Fabrication of Efficient Low-Bandgap Perovskite Solar Cells by Combining Formamidinium Tin Iodide with Methylammonium Lead Iodide," *J. Am. Chem. Soc.*, vol. 138, no. 38, pp. 12360–12363, 2016, doi: 10.1021/jacs.6b08337.

[14] T. Wang *et al.*, "Highly Air-Stable Tin-Based Perovskite Solar Cells through Grain-Surface Protection by Gallic Acid," *ACS Energy Lett.*, vol. 5, no. 6, pp. 1741–1749, Jun. 2020, doi: 10.1021/acsenergylett.0c00526.

[15] C. Ran *et al.*, "Conjugated Organic Cations Enable Efficient Self-Healing $FASnI_3$ Solar Cells," *Joule*, vol. 3, no. 12, pp. 3072–3087, 2019, doi: 10.1016/j.joule.2019.08.023.

[16] N. Ghimire *et al.*, "Mitigating Open-Circuit Voltage Loss in Pb-Sn Low-

Bandgap Perovskite Solar Cells via Additive Engineering," *ACS Appl. Energy Mater.*, vol. 4, no. 2, pp. 1731–1742, 2021, doi: 10.1021/acsaem.0c02895.

[17] Y. Sun *et al.*, "Preferred Film Orientation to Achieve Stable and Efficient Sn-Pb Binary Perovskite Solar Cells," *ACS Appl. Mater. Interfaces*, vol. 13, no. 9, pp. 10822–10836, 2021, doi: 10.1021/acsami.0c19014.

[18] K. Nishimura *et al.*, "Lead-free tin-halide perovskite solar cells with 13% efficiency," *Nano Energy*, vol. 74, p. 104858, 2020, doi: 10.1016/j.nanoen.2020.104858.

[19] G. Xie, L. Xu, L. Sun, Y. Xiong, P. Wu, and B. Hu, "Insight into the reaction mechanism of water, oxygen and nitrogen molecules on a tin iodine perovskite surface," *J. Mater. Chem. A*, vol. 7, no. 10, pp. 5779–5793, 2019, [Online]. Available: http://xlink.rsc.org/?DOI=C8TA11705E.

[20] B. Subedi *et al.*, "Urbach Energy and Open-Circuit Voltage Deficit for Mixed Anion-Cation Perovskite Solar Cells," *ACS Appl. Mater. Interfaces*, 2021, doi: 10.1021/ACSAMI.1C19122/SUPPL_FILE/AM1C19122_SI_001.PDF.

[21] A. Rajagopal, P. W. Liang, C. C. Chueh, Z. Yang, and A. K. Y. Jen, "Defect Passivation via a Graded Fullerene Heterojunction in Low-Bandgap Pb-Sn Binary Perovskite Photovoltaics," *ACS Energy Lett.*, vol. 2, no. 11, pp. 2531–2539, 2017, doi: 10.1021/acsenergylett.7b00847.

[22] G. Kapil *et al.*, "Strain Relaxation and Light Management in Tin-Lead Perovskite Solar Cells to Achieve High Efficiencies," *ACS Energy Lett.*, vol. 4, no. 8, pp. 1991–1998, 2019, doi: 10.1021/acsenergylett.9b01237.

[23] A. Kojima, K. Teshima, Y. Shirai, and T. Miyasaka, "Organometal halide perovskites as visible-light sensitizers for photovoltaic cells," *J. Am. Chem. Soc.*, vol. 131, no. 17, pp. 6050–6051, 2009, doi: 10.1021/ja809598r.

[24] W. A. Laban and L. Etgar, "Depleted hole conductor-free lead halide iodide heterojunction solar cells," *Energy Environ. Sci.*, vol. 6, no. 11, pp. 3249–3253, 2013, doi: 10.1039/c3ee42282h.

[25] L. Etgar *et al.*, "Mesoscopic CH 3NH 3PbI 3/TiO 2 heterojunction solar cells," *J. Am. Chem. Soc.*, vol. 134, no. 42, pp. 17396–17399, 2012, doi: 10.1021/ja307789s.

Chapter 6 Conclusions and Recommendations

This chapter illustrates the experimental work performed to prepare the mixed Sn-Pb halide precursors, substrate preparation and the fabrication of the perovskite films. In addition, it also describes the parameters used to characterize these films.

6.1 Conclusions

In this research work, the role of caff. (1,3,7-trimethylpurine-,2,6-dione) molecule containing two C=O functional groups for the ambient fabrication of $FA_{0.2}MA_{0.8}Sn_{0.5}Pb_{0.5}I_{2.4}Br_{0.6}$ narrow bandgap perovskite absorber films in a low humidity environment (RH< ~10%). The C=O functional groups in the caff. act as an electron-donating Lewis-base reacting with Pb^{2+} and Sn^{2+} ions to form an intermediate adduct modulating the fast crystallization of Sn-Pb mixed perovskite films. The $FA_{0.2}MA_{0.8}Sn_{0.5}Pb_{0.5}I_{2.4}Br_{0.6}$ perovskite absorber films are prepared with different concentration ratios of caff. (0 mol%, 1.25 mol%, 2.5 mol%, and 5 mol%). Among them, 1.25 mol% caff. doped perovskite absorber films show the most optimum structural, morphological, and optoelectronic properties in comparison to others. Moreover, all the prepared Sn-Pb mixed perovskite absorber films show E_u values higher than 200 meV attributed to the easy oxidation of Sn^{2+} with a maximum E_u value of 273 meV for control and a minimum E_u value of 229 meV for 1.25 mol% caff. doping concentration. In short, acid-base adduct formation has proved a significant tool to regulate fast crystallization of Sn-Pb mixed perovskite absorber films in ambient environment. We hope this work will endeavour the development of Sn-Pb based PSCs in ambient conditions.

6.2 Future Recommendations

For the future work, the following suggestions are recommended to fabricate a complete working device in ambient conditions based on the Sn-Pb mixed perovskites:

1. Passivation of surface defects: Facile Sn^{2+} oxidation initiates from the surface and proceeds to the bulk of the Sn-Pb mixed perovskite films. To prevent this, it is recommended to passivate uncoordinated Sn^{2+} present at the surface of the Sn-Pb mixed perovskites films to avoid formation of defect states.

2. Passivation of bulk defects: As a consequence of the Sn^{2+} in ambient environment, bulk oxidation of Sn-Pb mixed perovskites take place ultimately loosing the perovskite structure. Therefore, it recommended to apply surface and defect passivation simultaneously to in Sn-Pb mixed perovskite to sustain their optoelectronic properties.
3. Fabrication of a Sn-Pb mixed PSCs in ambient environment: To study the effect of caff. doping on the complete device performance, it is recommended to fabricate a complete perovskite solar cell in future.

Appendix-A: Journal Article

Carbonyl functional group assisted crystallization of mixed tin-lead narrow bandgap perovskite absorber in ambient conditions

Abdul Sattar[a], Nadia Shahzad[a], Muhammad Ali Tariq[a], Tanzeela Yousaf[a], Muhammad Salik Qureshi[a], Muhammad Imran Shahzad[b], Rabia Liaquat[a], Majid Ali[a]

AFFILIATIONS

[a] U.S Pakistan Center for Advanced Studies in Energy (USPCAS-E), National University of Sciences and Technology (NUST), H-12, Islamabad, Pakistan.

[b] Nanoscience & Technology Department (NS&TD), National Centre for Physics (NCP), 44000-Islamabad, Pakistan.

ABSTRACT

Tin-lead (Sn-Pb) perovskite solar cells are receiving growing interest due to their applications in tandems and lead mitigation. Nonetheless, fast crystallization and facile Sn^{2+} oxidation restrict their ambient fabrication which increases fabrication costs. This letter presents an experimental study on additive assisted growth of $FA_{0.2}MA_{0.8}Sn_{0.5}Pb_{0.5}I_{2.4}Br_{0.6}$ narrow bandgap perovskite films employing a Lewis-base molecule, caffeine (1,3,7-trimethylpurine-,2,6-dione), having two carbonyl functional groups (C=O) in a low humidity environment (<~10%). The C=O interacts with metallic ions (Sn^{2+} and Pb^{2+}) via chelation to form an acid-base adduct, slowing down the fast crystallization of $FA_{0.2}MA_{0.8}Sn_{0.5}Pb_{0.5}I_{2.4}Br_{0.6}$ perovskite films. As a result, the grain size improves resulting in better structural and optical properties. In contrast, Urbach energy values showed higher electronic disorder near the band edges even upon caffein doping implying Sn^{4+} doping in ambient environment. This work accentuates the potential of the acid-base adduction to regulate uncontrolled crystallization of Sn-Pb perovskites in ambient environment.

Keywords: *Ambient fabrication, Tin-Lead mixed perovskites, Narrow bandap, Lead mitigation*

Submitted To: Journal of Applied Physics Letters

Appendix-B: Journal Article

Unravelling the Role of Bifunctional Additives Towards Realization of Highly Efficient and Environmentally Robust Tin Halide Perovskite Solar Cells

Abdul Sattar[1], Nadia Shahzad[1], Muhammad Ali Tariq[1], Tanzeela Yousaf[1], Muhammad Imran Shahzad[2], Rabia Liaquat[1], Majid Ali[1], Zuhair S. Khan[1], Federico Bella[3]*

[1] U.S Pakistan Center for Advanced Studies in Energy (USPCAS-E), National University of Sciences and Technology (NUST), H-12, Islamabad, Pakistan.

[2] Nanoscience & Technology Department (NS & TD), National Centre for Physics (NCP), 44000-Islamabad, Pakistan.

[3] Department of Applied Science and Technology, Politecnico di Torino, Corso Duca degli Abruzzi 24, 10129 Torino, Italy

ABSTRACT

Tin halide perovskite (THP) materials have become a popular choice as lead-free perovskites for solar cell applications owing to their narrow bandgap, high charge carrier mobilities, and low-exciton binding energies. However, tin halide-based perovskite solar cells (TH-PSCs) performance and stability are primarily hampered by the volatile nature of tin (II) in the ambient environment and uncontrolled crystallization at room temperature. For quite some time, tin halides and metallic tin have been used as tin (Sn^{2+}) compensators in TH-PSCs. Still, the performance of TH-PSCs has not improved significantly due to the phase segregation produced by tin-based additives, endangering the morphology of THP films. Recently, bifunctional additives (BAs) containing different functional groups have promised tremendous potential to alleviate Sn^{2+} oxidation and prohibit fast crystallization.

Keywords: *Tin oxidation, Fast crystallization, Bifunctional additive, Tin halide perovskite solar cells*

Submitted To: Journal of Energy and Environmental Materials